이학박사 학위논문

Aquaporin-4 경로를 통한 뇌혈관 장벽 보호 및 출혈 주변 부종 개선 효과에 관한 연구

Upregulation of AQP4 improves blood-brain barrier integrity and perihematomal dema following intracerebral hemorrhage

울 산 대 학 교 대 학 원

의 과 학 과

전 한 울

Aquaporin-4 경로를 통한 뇌혈관장벽 보호 및 출혈 주변 부종 개선 효과에 관한 연구

지 도 교 수 이 승 주

이 논문을 이학박사 학위 논문으로 제출함

2021년 11월

울 산 대 학 교 대 학 원
의 과 학 과
전 한 울

전한울의 이학박사 학위논문을 인준함

심사위원 박 원 형 (인)

심사위원 이 승 주 (인)

심사위원 이 은 재 (인)

심사위원 이 준 엽 (인)

심사위원 조 성 우 (인)

울 산 대 학 교 대 학 원

2022년 2월

Abstract

In intracerebral hemorrhage (ICH), delayed secondary neural damages largely occur from perihematomal edema (PHE) resulting from the disruption of the blood–brain barrier (BBB). PHE is often considered the principal cause of morbidity and mortality in patients with ICH. Nevertheless, the main cellular mechanism as well as the specific BBB component involved in the formation of PHE after ICH remains elusive. Herein, we evaluated the role of AQP4, a water channel expressed on the astrocytes of the BBB, in the formation of PHE in ICH. The static and dynamic functions of the BBB were evaluated by analyzing the microstructure and leakage assay. Protein changes in the PHE lesion were analyzed and the control mechanism of AQP4 expression by reactive oxygen species was also investigated. Delayed PHE formation due to BBB disruption after ICH was confirmed by the decreased coverage of multiple BBB components and increased dynamic leakages. Microstructure assay showed that among the BBB components, AQP4 showed a markedly decreased expression in the PHE lesions. The decrease in AQP4 was due to microenvironmental ROS derived from the hemorrhage and was restored by treatment with ROS scavenger. AQP4-deficient mice had significantly larger PHE lesions and unfavorable survival outcomes compared with wild-type mice. Our data identify AQP4 as a specific BBB-modulating target for alleviating PHE in ICH. Further comprehensive studies are needed to form the preclinical basis for the use of AQP4 enhancers as BBB modulators for preventing delayed cerebral edema after ICH.

Keywords: Perihematomal edema, Vasogenic edema, Intracerebral hemorrhage, Vascular biology

Contents

Figure contents

Abbreviations

AQP4	Aquaporin-4
BV	Blood vessel
BBB	Blood-brain barrier
CaM	Calmodulin
CNS	Central nervous system
DHE	Dihydroethidium
EED	Edema extension distance
ETbR	Endothelin B receptor
GFAP	Glial fibrillary acidic protein
H_2O_2	Hydrogen peroxide
ICH	Intracerebral hemorrhage
NAC	N-acetylcysteine
PHE	Perihematomal edema

Chapter 1. Introduction

Increases in BBB permeability in delayed cerebral edema after an intracerebral hemorrhage lead to significant morbidity and exacerbate clinical outcomes [1-3]. Nevertheless, the mechanism of the delayed increase in BBB permeability is mostly unknown, and the specific component of the BBB microenvironment involved in the formation of cerebral edema in intracerebral hemorrhage is yet to be identified [4]. Due to the cessation of blood supply, the movement of fluids after cerebral infarction is largely driven without energy support. As a result, the progressive changes in osmotic and hydrostatic conductivity of abnormal capillaries could be categorized into three phases: formation of ionic edema due to Na^+-K^+ channel failure, formation of vasogenic edema due to ischemia-induced capillary failure, and catastrophic failure with hemorrhagic transformation. Cytotoxic edema, or cellular swelling, manifests minutes after acute injuries to the central nervous system (CNS). Ionic edema, which refers to extracellular edema occurring in the presence of intact blood-brain barrier (BBB), forms immediately following cytotoxic edema. Vasogenic edema, which is extracellular edema that includes the extravasation of plasma proteins, manifests hours after the initial insult [3, 4]. The BBB permeability is canonically regulated by alterations in endothelial tight junctions and PDGFR-beta-controlled pericyte coverage[5, 6]; however, it is unclear whether these mechanisms also play a major role in the formation of PHE. To date, 13 members of the AQP family have been discovered [7, 8], among which AQP4 is specifically localized at astrocyte surfaces of the blood-brain- and cerebrospinal fluid-brain barriers [9]. AQPs are historically known to be passive transporters of water. However, the accumulated evidence in the last decade has highlighted the diverse function of AQPs beyond water homeostasis. For example, emerging biophysical evidence suggests that AQPs may also facilitate gas (CO2) and cation transport. In addition, AQPs may be involved in the cell signaling for volume regulation and controlling the subcellular localization of other proteins by forming

macromolecular complexes. Moreover, a subgroup of AQP water channels also facilitates transmembrane diffusion of small, polar solutes, water, and aquaglyceroporin [8, 10-12]. AQP1 is expressed in the apical membrane of choroid plexus epithelium and showed a protective role in hypertensive rats [13]. Conversely, AQP11 is expressed on brain endothelial cells and induces PHE, an effect associated with miR-27a-3p [14]. Importantly, AQP4 acts as a Janus-like water channel in cerebral edema formation [15], as it allows bidirectional flux of water through the cell membranes and facilitates water transport to and from the brain parenchyma[16]. Accordingly, both genetic deletion and overexpression of AQP4 have been shown to increase water accumulation in the brain after cerebral infarction and hemorrhage[17-19]. They are suggesting that the disease-specific microenvironment regulates the net function of AQP4 in cerebral edema. Thus, a targeted study is needed to identify the regulators of AQP4 expression in pathological conditions and determine if targeting the AQP4 regulator may confer clinical benefits in intracerebral hemorrhage. Edema is a hallmark of secondary CNS injuries after ischemic stroke or hemorrhage, and it is mainly mediated by AQP4. Targeting the subcellular localization of AQP4 in ischemia and hypoxia not only alleviates edema but also stabilizes the BBB or BSCB, thus leading to improved functional outcomes as shown in studies with CaM or PKA inhibition. Moreover, a recent study showed that targeting AQP4 reduces cerebral edema during the early post-stroke phase in mice. Although the above studies convincingly demonstrated the role of AQP4 in the early phase of cytotoxic edema, the role of AQP4 in vasogenic edema is still elusive. Therefore, we focused on the role of AQP4 in the delayed PHE formation by vasogenic edema after intracerebral hemorrhage [20, 21]. Herein, we investigated the significance of AQP4 in intracerebral hemorrhage as well as the therapeutic role of ROS scavenger as a microenvironmental modulator of AQP4 using animal models.

Chapter 2. Material and Methods

2.1 Animal experiments

All animal experiments in this study were conducted under the approval and guideline of the Institutional Animal Care and Use Committee (IACUC) of Asan Institute for Life Sciences in Asan Medical Center. C57BL/6 mice (OrientBio, Seongnam-si, Gyeonggi-do, Republic of Korea) and aquaporin-4 knock-out ($AQP4^{-/-}$) mice (RIKEN, Saitama, Japan) at 7–10 weeks of age were used for experiments. To generate an intracerebral hemorrhage murine model, 50 μl of autologous blood collected from the retroorbital venous plexus was infused into the basal ganglia (coordinates: 2.0 mm (right), 0.2 mm (anterior), 3.7 mm (depth) apart from bregma) under general anesthesia with an intraperitoneal injection of ketamine (100 mg/kg) and xylazine hydrochloride (10 mg/kg); the infusion rate was continuously controlled at a rate of 1.25 μl/min by an automated infusion system (Hamilton, Boston, MA, USA) [22]. T2-weighted magnetic resonance images (Bruker Pharmascan 9.0T/160 mm, Ettlingen, Germany) were acquired on days 1, 3, and 7 after intracerebral hemorrhage induction. The parameters of MRI were as follows: repetition time = 4500.00 ms, echo time = 50.00 ms, averages = 2, echo spacing = 16.667 ms, matrix size = 256*256, slice thickness = 0.5 mm. The sizes of the hematoma and PHE were measured using the Image J software (NIH, Bethesda, MD, USA) and calculated using the equation shown below[23]:

$$\text{EED (Edema extension distance)} = \sqrt[3]{\frac{\text{Edema volume + Hemorrhage volume}}{4/3 \text{ X } \pi}} - \sqrt[3]{\frac{\text{Hemorrhage volume}}{4/3 \text{ X } \pi}}$$

Since EED (Edema Extension Distance) is not affected by hematoma size and reflects PHE change well, the PHE change was analyzed using EED. Therefore, the EED was calculated as follows [24, 25]. ROS scavenger (N-acetylcysteine[26], Catalog No: A7250, 200 mg/kg; Sigma), 6-hydroxy-2,5,7,8-tetramethylchroman-2-carboxylic acid (Trolox [27], Catalog No: 238813, 100 mg/kg; Sigma), functionally AQP4-enhancing substance (BQ-788 sodium salt [28], Catalog No:

1500, 3 mg/kg; Tocris Bioscience), and aquaporin inhibitor (2-nicotinamide-1,3,4-thiadiazole (TGN-020 [29], Catalog No: SML0136, 100 mg/kg; Sigma) were administered every other day for 14 days via intraperitoneal injection.

2.2 Immunofluorescence staining and histologic analysis

The microstructures and dynamic leakages of BBB in PHE were investigated after intracerebral hemorrhage induction. The vascular structures were visualized by CD31 staining and lectin perfusion (DyLight-649 labeled lectin, Catalog No: DL-1178-1, 0.1 mg/mouse, Vector Laboratories). To assess the BBB leakage, Evans blue (Sigma, Catalog No: E2129, 2% in PBS) and dextran 10-kDa (Invitrogen, Catalog No: D1817) were each perfused for 12 hrs and 5 mins prior to sacrifice. The brain tissue was fixed in two steps: perfusion with 4% paraformaldehyde for 5 mins via the trans-cardiac route for pre-harvest fixation, and immersion in 4% paraformaldehyde for 24 hrs for post-harvest fixation. The fixed samples were serially dehydrated in 10% to 30% sucrose solutions for 24 hrs at each concentration. The fully prepared samples were sliced at a thickness of 60 μm followed by permeabilization with 0.3% triton x-100 in phosphate-buffered saline solution for 10 mins. To prevent non-specific antibody binding, the samples were blocked using 1% bovine serum albumin for 30 mins. The samples were then treated with primary antibodies against the BBB components and incubated overnight in a cooling chamber. The primary antibodies used are as follows: CD13 and PDGFR-beta for pericytes; laminin for basement membrane; GFAP and S100-beta for activated astrocytes; aquaporin-4; and CD31 for endothelial cells. Fluorescence-tagged secondary antibodies were selected according to the species of the primary antibodies. DAPI was used for nuclear staining. The fluorescence images were acquired using LSCM 710 (Zeiss) and processed with the ZEN image software (Zeiss). For detection of specific proteins, the following antibodies and reagents were used: CD31 (BD Biosciences, Catalog No: 550274, 1:100; Merck, Catalog No: MAB1398Z; 1:100), PDGFR-

beta (ebioscience, Catalog No: 14-1402-82, 1:100), GFAP (NOVUS, Catalog No:NB300-141,1:1000), AQP4(SANTACRUZ, Catalog No:SC-32739, 1:100 and allomone labs, Catalog No:AQP-004, 1:100), VE-cadherin (BD biosciences, Catalog No: 555289, 1:100), Claudin-5 (Invitrogen, Catalog No:35-2500, 1:200), Laminin (Sigma-Aldrich, Catalog No:L9393, 1:250), Ter119(ebioscience, Catalog No: 14-5921-82, 1:100) and fluorescent conjugated secondary antibody (Bethyl, Donkey anti-goat FITC Catalog No: A50-101F; Donkey anti-goat Dylight 550, Catalog No:A50-101D3; Donkey anti-mouse FITC, Catalog No: A90-137F; Donkey anti-mouse Dylight 550, Catalog No: A90-137D3; Donkey anti-rabbit FITC, Catalog No: A120-108F; Donkey anti-rabbit Dylight 550, Catalog No: A120-108D3; biolegend, Goat anti-hamster Alexa 488, Catalog No: 405503; Goat anti-hamster Dylight 594, Catalog No: 405504; all secondary antibody dilutions:, 1:500).The parameters of laser scanning confocal microscopy and numerical aperture of the utilized lens are as follows.

Objective lens	20x/0.80 M27
	63x/1.2W
Dimensions	1024x1024
Pinhole	88 μm
Laser power	405 nm: 3.5%
	488 nm: 35%
	561 nm: 45%
	633 nm: 50%
Filters	Ch1: 410-480
	ChS1: 495-553
	ChS2: 563-650
	Ch2: 660-719
Refractory index	1.46

2.3 Three-dimensional blood vessel analysis

Three-dimensional images around the hematoma and edema were obtained instead of two-dimensional images to minimize the artifacts in measuring the BBB leakage. Before sacrifice, the mice were perfused with 488-lectin via the trans-cardiac route for 5 mins and fixed according to the protocol mentioned earlier. The harvested samples were sliced at a thickness of 3 mm to fully include the lesion sites, followed by tissue clearing with the Binaree Tissue Clearing™ Kit (Binaree, Catalog No: HRTC-001) for 24 hrs in a warm bath. After the clearing process, the samples became transparent enough for the lasers to pass through. The transparent samples were adjusted to a refractive index of 1.45 by immersion in a mounting solution for 24 hrs. After embedding in low gelling temperature agarose (Sigma, Catalog No: A9414, 1% in distilled water), three-dimensional images were obtained using light-sheet microscopy (Z.1, Zeiss) with the following acquisition parameters: magnification = 5×/0.16, exposure time = 99.9 ms, zoom factor = 0.7. The acquired images were processed using ZEN image software (Zeiss).

2.4 *In vitro* experiments

Human astrocytes (Sciencell, Catalog No: 1800) and human brain endothelial cells (HBEC-5i, ATCC) were co-cultured in an *in vitro* system to recapitulate the astrocyte coverage around the vessels. Before co-culture, the astrocytes and endothelial cells were each incubated in astrocyte media (Sciencell, Catalog No: 1801) and endothelial cell growth media (Promocell, Catalog No: C-22010). The top surface of the polyester membrane (Corning) was coated with poly-L-lysine (Sigma, Catalog No: P6282) for 2 hours. The bottom surface was coated with 0.1% gelatin in cell culture water (Sigma, Catalog No: G1393) for 2 hrs. Astrocytes and endothelial cells were seeded and stabilized sequentially for 2 hrs and then incubated for 48 hrs[30]. In the ROS treatment experiment, 50 μM and 100 μM of hydrogen peroxide (H_2O_2) (MPbio, Catalog No: 7722-84-1)

were added to the co-culture media; then, 100 μM of the ROS scavenger N-acetylcysteine (Sigma, Catalog No: A7250) was treated for 4 hrs and replaced once every hour. Then, the co-cultured astrocytes and endothelial cells were washed and fixed with 4% cold paraformaldehyde and collected for Western blot and immunofluorescence analysis.

2.5 Protein analysis

The PHE region in mice was microdissected and lysed in 0.5% PBS-T (Triton X-100) solution. According to the manufacturer's protocol, protein levels were quantified using the cytokine protein array kit (RayBiotech C2000, Catalog No: AAM-CYT-2000). Human astrocytes were lysed in RIPA lysis buffer (ENZO Life sciences, Catalog No: ADI-80-1284) containing phosphatase inhibitor cocktail (Sigma, Catalog No: P5726 and P0044) and proteinase inhibitor cocktail (Roche, Catalog No: 11697498001). The cell lysates' protein concentration was determined by bicinchoninic acid assay (Thermo Fisher Scientific, Catalog No: 23227), and the cell lysates were then resolved in SDS-PAGE gels. For detection of specific proteins, the following antibodies were used: AQP4 (allomone labs, Catalog No: AQP-004, 1:1000), Beta-actin (SANTA CRUZ, Catalog No: sc-47778, 1:1000), total Akt (Cell signaling, Catalog No:9272, 1:1000), p-Akt (Cell signaling, Catalog No: 9271, 1:1000), total FoxO3a (Cell signaling, Catalog No: 2497, 1:1000), p-FoxO3a (Cell signaling, Catalog No: 9466, 1:1000), p-Erk (Cell signaling, Catalog No: 4376, 1:1000), and total Erk (Cell signaling, Catalog No: 9102, 1:1000). Western blotting analysis was performed according to standard procedures, and the protein signals were developed by the enhanced Amersham ECL western blotting analysis system (GE Healthcare, Catalog No: RPN2232).

2.6 Reactive oxygen species analysis

After ICH, PHE areas of the brain specimens were obtained after MRI and used collagenase/Dispase enzyme (Roche, Catalog No: 10269638001) to digest tissues before single-cell isolation. After digestion, Cells were passed through a 40um cell strainer, and myelin and cell debris were removed by 22% percoll (Sigma, Catalog No: P4937) gradient centrifugation. Single cells were resuspended in 2% FBS in PBS buffer and labeled with Cellrox-FITC (Invitrogen, Catalog No: C10444), CD31-APC/Fire 750 (Biolegend, Catalog No: 102528, 1:500) antibodies. For intracellular staining, single cells were permeabilized and fixed with BD Cytofix/cytoperm Fixation/Permeabilization Kit (BD Biosciences, Catalog No: 554714) after surface staining. The cells were washed twice with 1× perm/wash buffer and stained with NeuN-PE (NOVUS, Catalog No: NBP1-92693PE, 1:500), GFAP-647 (BD biosciences, Catalog No: 561470, 1:500). Flow cytometry data were obtained from BD FACS canto ii workstation (BD biosciences) and analyzed using Flow jo software.

2.7 Inclusion and exclusion criteria

Inclusion and exclusion criteria are addressed below.

2.7.1 Inclusion criteria

1) C57/B6 male mice with age 8~10 weeks, female mice were excluded due to the effect of hormonal variations

2) Purchased from Orient bio co. and adapted in inbreed facility

3) Healthy without evidence of hypertension, anemia, vasculopathy, and neurological deficiency

4) Mice survived after intracerebral hemorrhage induction at immediate post-procedure period

5) Mice successfully weaned from anesthesia

2.7.2 Exclusion criteria

1) Profound hemorrhage over expected intracerebral hemorrhage induction (secondary hemorrhage)

2) Mice with unexpected small intracerebral hemorrhage volume (model production failure)

3) Brain death or imminent death after procedure

4) Seizure requiring acute management

5) Post-cardiac arrest with suspected significant anoxic brain injury

2.8 Randomization and Blinding

After screening, eligible mice were randomly allocated to the control group or ROS scavenger group (N-acetylcysteine, BQ-788 each) in a 1:1 ratio using an interactive web response system. Allocation will be by randomly permuted blocks and stratified by hemorrhage size to enhance balance. Partial blinding was applied in the present study. The agents were not blinded because it was not feasible to manufacture and manage pseudo-drugs. However, procedural blinding was achieved with separate experiments. The researcher made a model that was not involved in radiologic measurements and analyses. Each mouse was assigned a unique number and measurement values were integrated by an independent researcher.

2.9 Sample size calculation

The primary endpoint for the study is the composite of survival outcome and perihematomal edema size at one week after randomization. We calculated the sample size by assuming that the primary endpoint rate would be 30% in the ROS scavenger group and that the edema reduction with ROS scavenger would be 40%. With 80% power and a one-sided level of significance of 0.05, 14 mice were required per treatment group. The software PASS version 12 (NCSS, LLC. Kaysville, Utah, USA) was used for the sample size calculation.

2.10 Statistical analysis

Values are reported as mean ± standard deviation unless indicated otherwise. For continuous data in animal studies, statistical significance was determined by the Mann-Whitney *U* test for comparison between two groups and the Kruskal-Wallis test with Bonferroni correction for comparison among multiple groups. The log-rank test was used for survival analysis. All statistical analyses were performed with PASW Statistics 18 (SPSS). Differences were considered to be statistically significant at $P < 0.05$.

Chapter 3. Results

3.1 Phenotypic analysis of the murine model of intracerebral hemorrhage

We generated a murine model of intracerebral hemorrhage by injecting 50 μl of autologous blood into the right basal ganglia, a region commonly affected by intracerebral hemorrhage (Fig. 1a). We investigated whether the model aptly recapitulates the PHE formation as observed in patients with intracerebral hemorrhage. We observed the chronological changes of PHE by T2-weighted MRI and found that the volume of PHE peaked at 3–4 days and resolved within 14 days (Fig 1b,c); similarly, the hematoma also resolved within 14 days. To evaluate the vascular permeability in the PHE, we systemically perfused the mice with Evans blue dye, which does not leak into the cerebral tissues in physiological conditions because multiple BBB components tightly cover the cerebrovascular structure. In our murine model of intracerebral hemorrhage, the Evans blue dye had leaked significantly in the PHE region (Fig. 2,3). Lectin perfusion assay also showed large amounts of leakage through the blood vessels, which showed characteristic dilation in the PHE region (Fig.4a,b).

To detect the protein changes in PHE, we performed multifaceted analysis on micro-capture dissection of the PHE region by using protein array and confocal microscopy. Among the proteins associated with BBB, AQP4 showed a markedly reduced expression in the PHE region (Fig. 5a and 5b). Confocal microscopy also showed that the widespread expression of AQP4 on the blood vessels in the normal brain was notably reduced in PHE rather than other BBB components (Fig. 6a-6e).

Genetically modified $AQP4^{-/-}$ mice showed a notably more rapid and widespread PHE formation as well as increased vascular leakage compared with wild-type mice (Fig. 7a). $AQP4^{-/-}$ mice also showed a significantly poorer survival following hemorrhage induction (Fig. 7b); moreover,

whereas wild type and AQP4$^{-/-}$ mice did not show a significant difference in the hematoma volume, the edema volume was significantly greater in AQP4$^{-/-}$ mice (Fig. 7c,7d). These results were recapitulated in pharmacological experiments using TGN-020, an AQP4 inhibitor (Fig. 8a,8b); compared with control mice without pharmacological treatment, mice treated with AQP4 inhibitors showed significantly delayed PHE resolution, increased PHE formation (Fig. 8c,8d,8e), increased vascular leakage (Fig. 9a, 9b), and reduced survival (Fig. 8f).

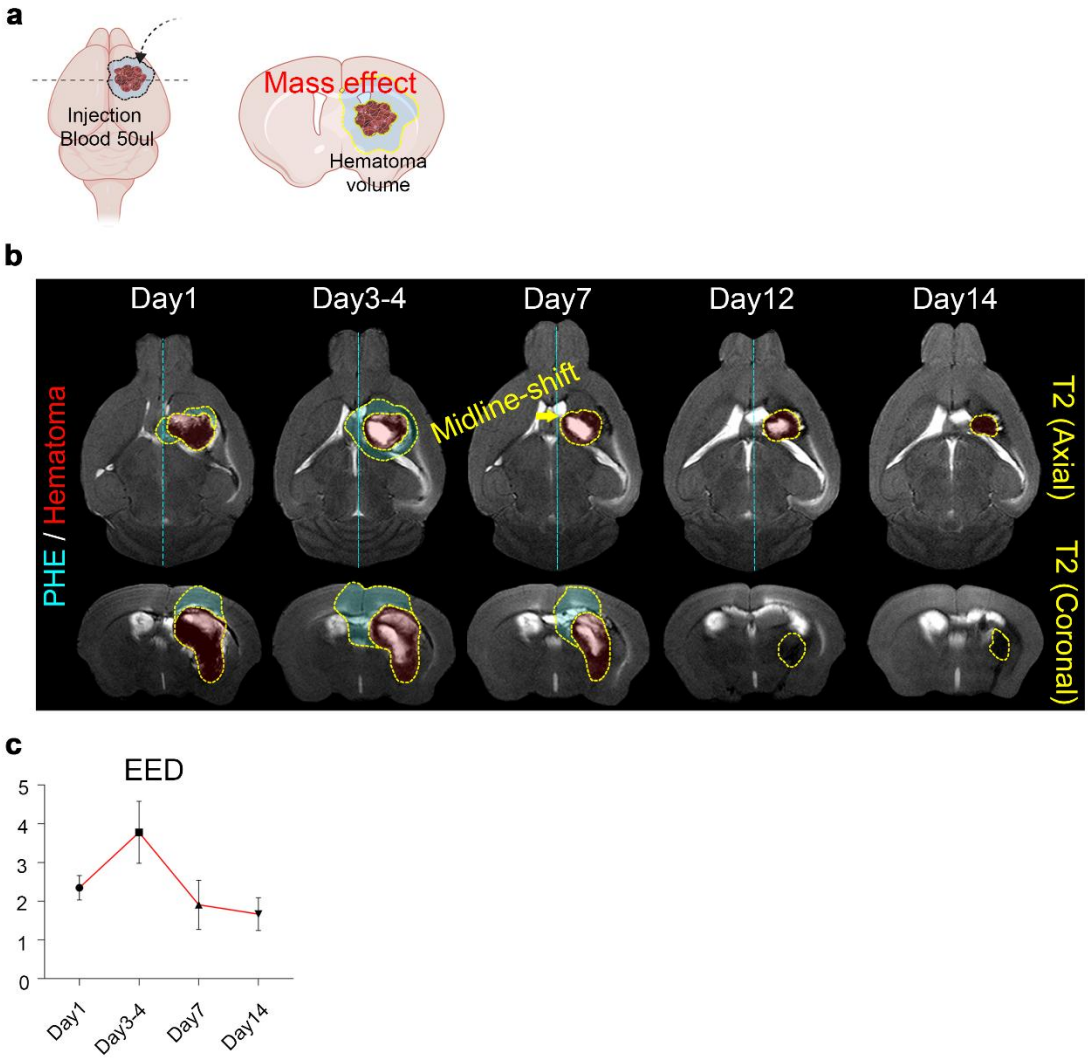

Figure 1. Phenotype after intracerebral hemorrhage in mouse model.

(a) Illustration depicting the generation of the animal model of intracerebral hemorrhage. (b) MR images showing the chronological changes in perihematomal edema (PHE) and hematoma in the intracerebral hemorrhage animal model. (c) Edema extension distance (EED) change in ICH mouse model

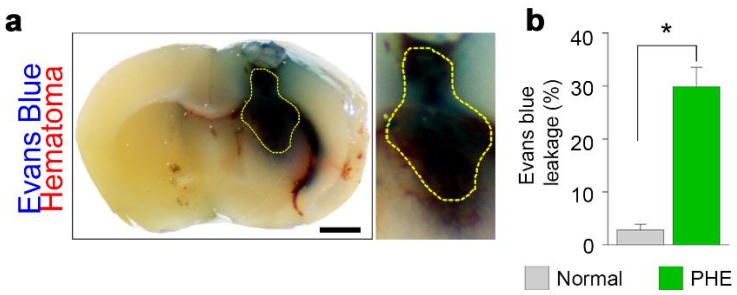

Figure 2. Evans blue (EB) extravasation after intracerebral hemorrhage.

(a) Representative gross image of coronal brain section showing Evans blue leakage. (b) Quantification of Evans blue extravasation intensity between experimental group. Leakage area intensity was calculated from the PHE area of the brain. ICH brain was compared to normal mouse brain. Data are mean ±SD. *$p<0.05$

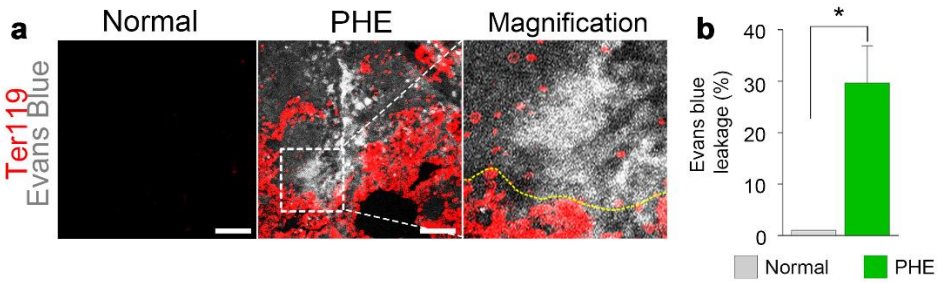

Figure 3. Leakage of Evans blue in perihematomal edema region.

(a) Immunofluorescence staining of Ter119+ red blood cells and Evans blue leakage in the PHE area (magnification x20). (b) Quantification of Evans blue extravasation fluorescence intensity between experimental group. Data are mean ±SD. *p<0.05

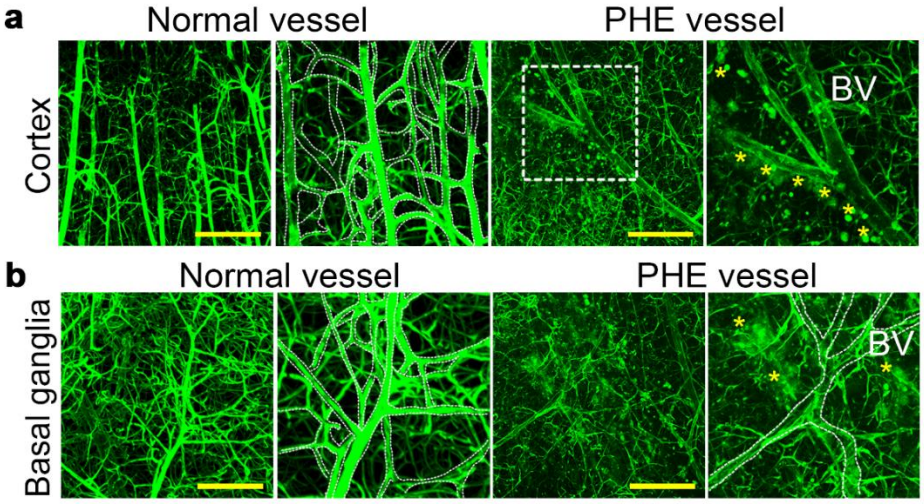

Figure 4. Three-dimensional fluorescence imaging of the hemorrhage vasculature.

(a) Lectin perfusion assay showing abnormal vasodilation and leakage in the cortex area in the PHE (b) Lectin perfusion assay showing leakage in the basal ganglia in the PHE (magnification x5); yellow scale bar, 200μm

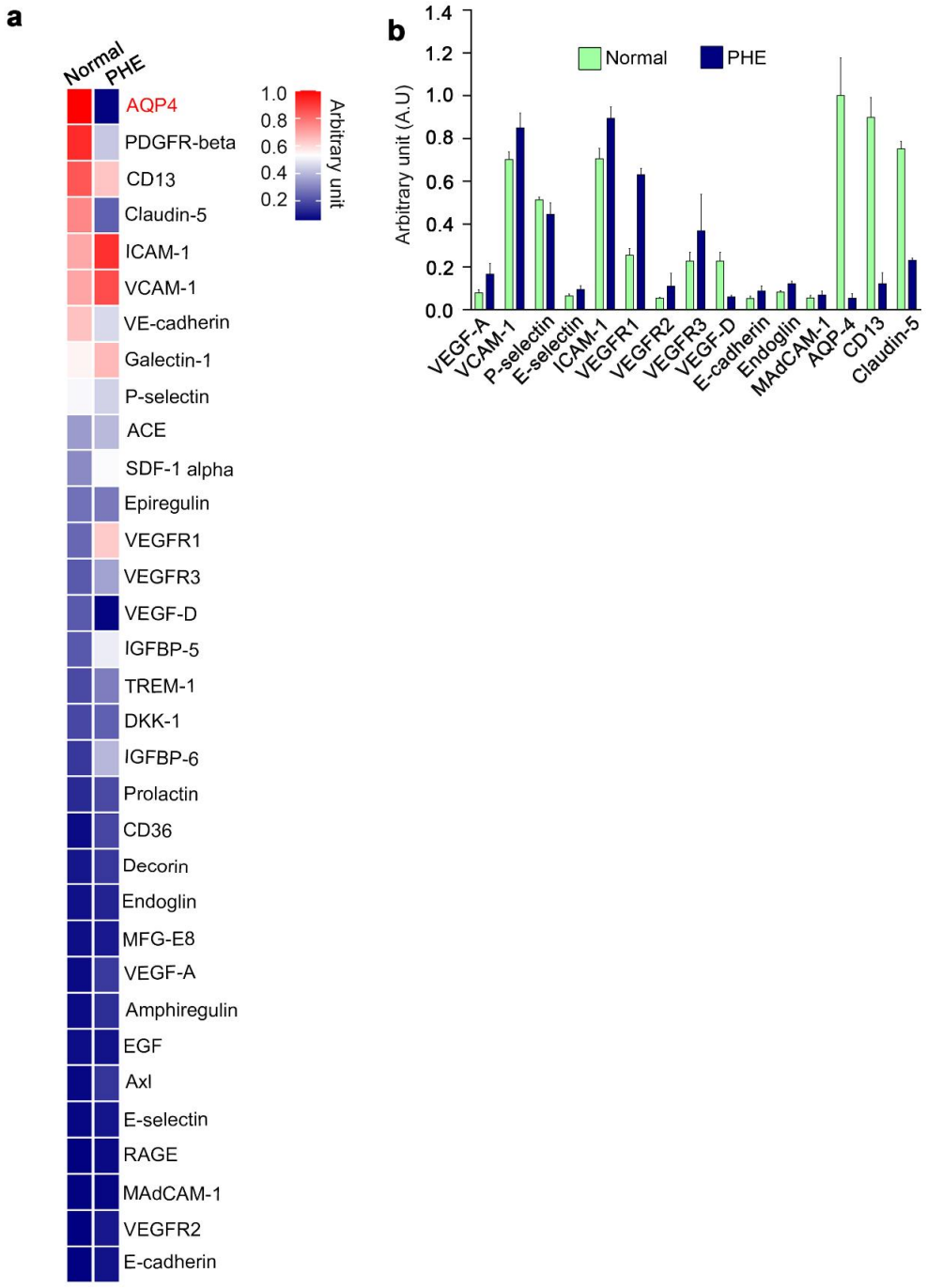

Figure 5. Proteomic changes in perihematomal edema brain tissue after intracerebral hemorrhage.

(a) Protein array of tissues from normal and PHE sites. (b) Quantification of vascular-associated proteins in the PHE region.

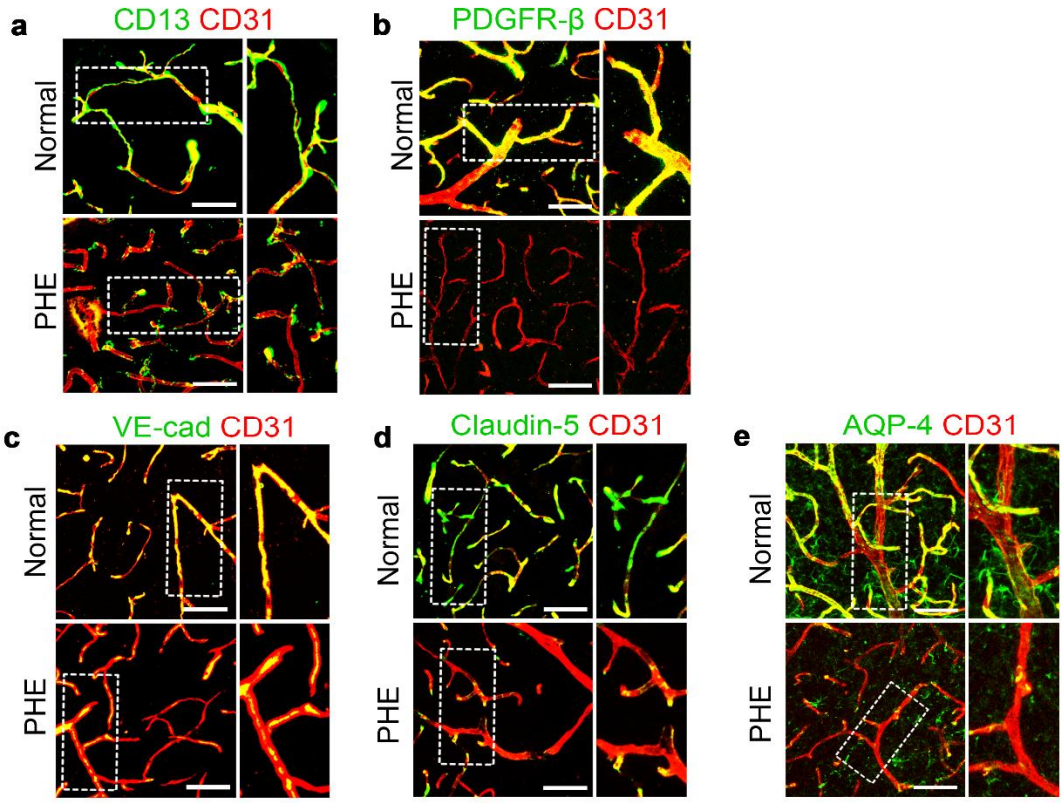

Figure 6. Blood-brain barrier disruption in perihematomal region after intracerebral hemorrhage.

Representative confocal images of vascular associated molecules in normal and PHE tissues (Magnification x20) (a) CD13 (b) PDGFR-beta (c) VE-cadherin (d) Claudin-5 (e) AQP-4.

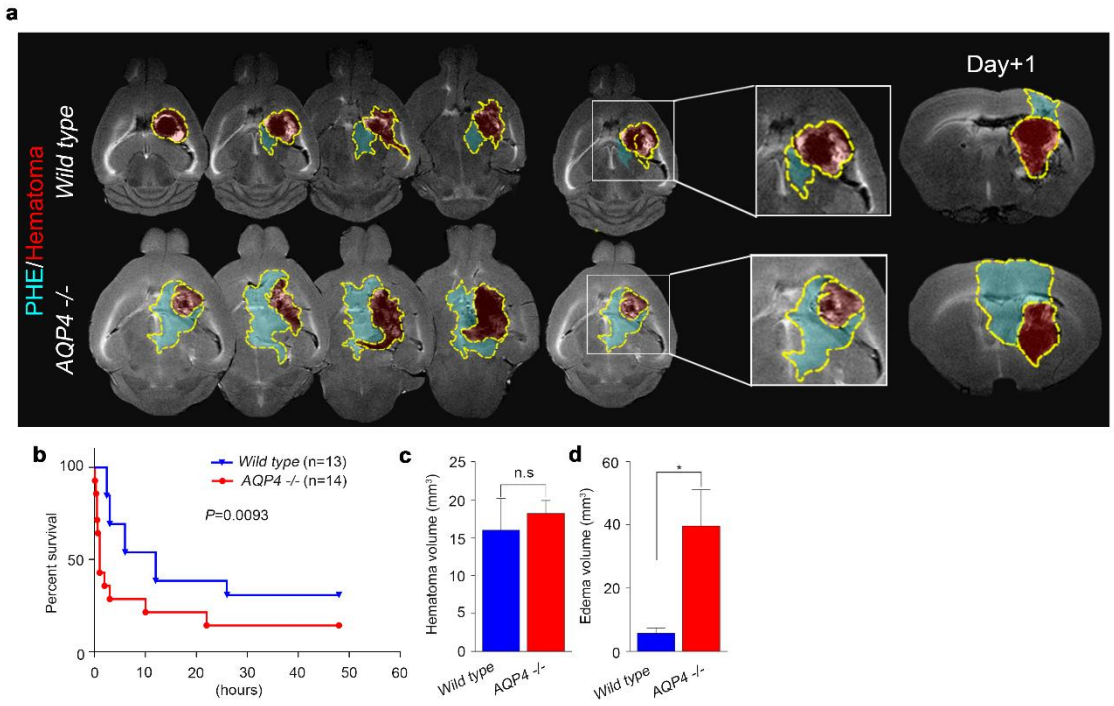

Figure 7. Comparison of edema formation and outcome in wild type and AQP4 $^{-/-}$ mice.

(a) MR images showing the chronological changes of PHE and hematoma in wild-type and AQP4$^{-/-}$ mice. (b) Survival curves of wild-type and AQP4 $^{-/-}$ mice after intracerebral hemorrhage. (c,d) Hematoma and edema volumes of wild-type and AQP4 $^{-/-}$ mice after intracerebral hemorrhage. Data are mean ±SD. *p<0.05

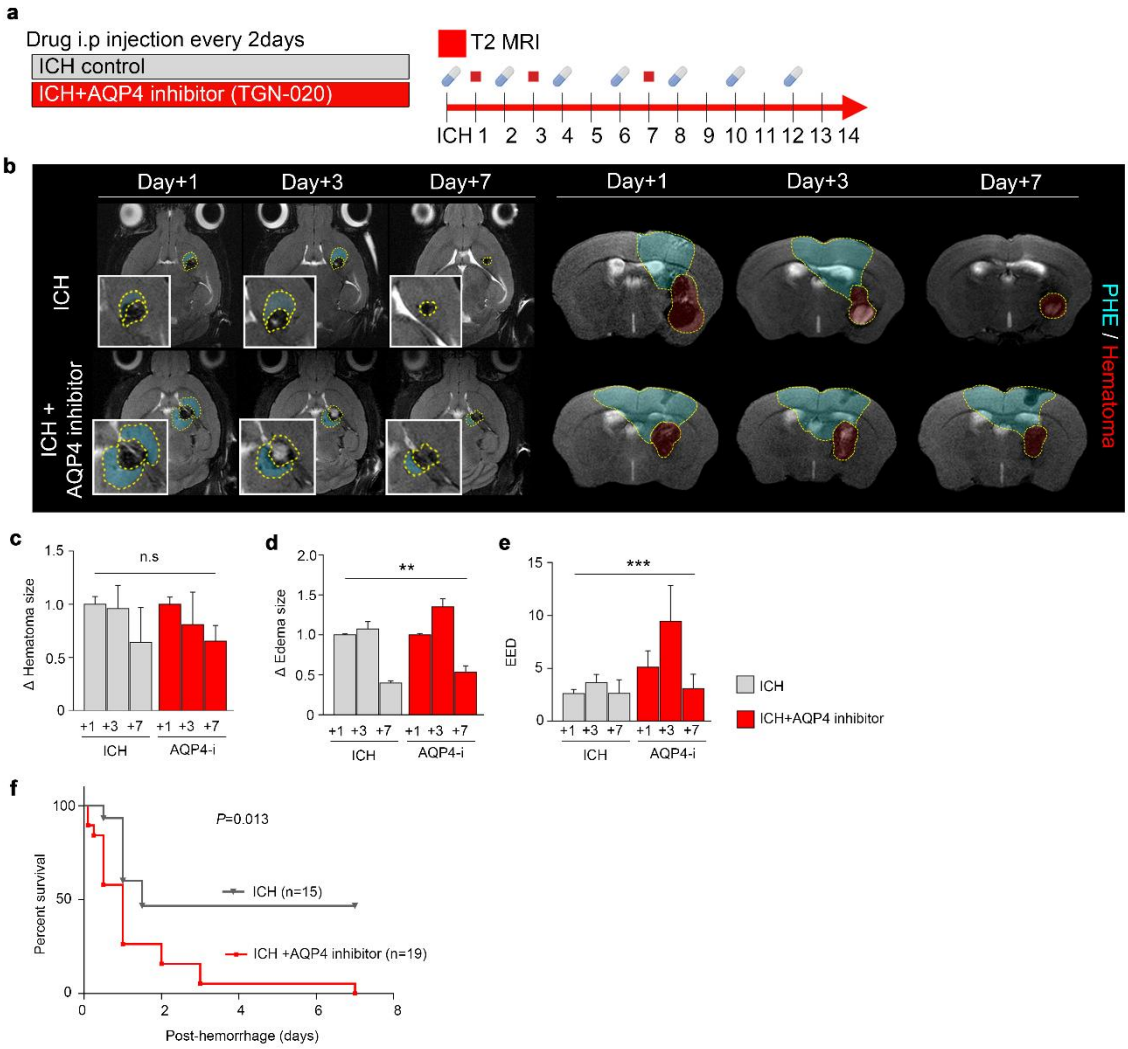

Figure 8. Delayed edema resolution after AQP4 inhibitor administration.

(a) AQP4 inhibitor (100mg/kg) was administered in animal models of intracerebral hemorrhage. (b) MR images taken at 1,3, and 7 days after intracerebral hemorrhage in mice treated with or without AQP4 inhibitor. (c,d,e) Quantification of the changes in the sizes of hematoma, edema and EED in T2WI of MRI (f) Survival curves of mice treated with or without AQP4 inhibitor after intracerebral hemorrhage. Data are mean ±SD. **p<0.01, ***p<0.001.

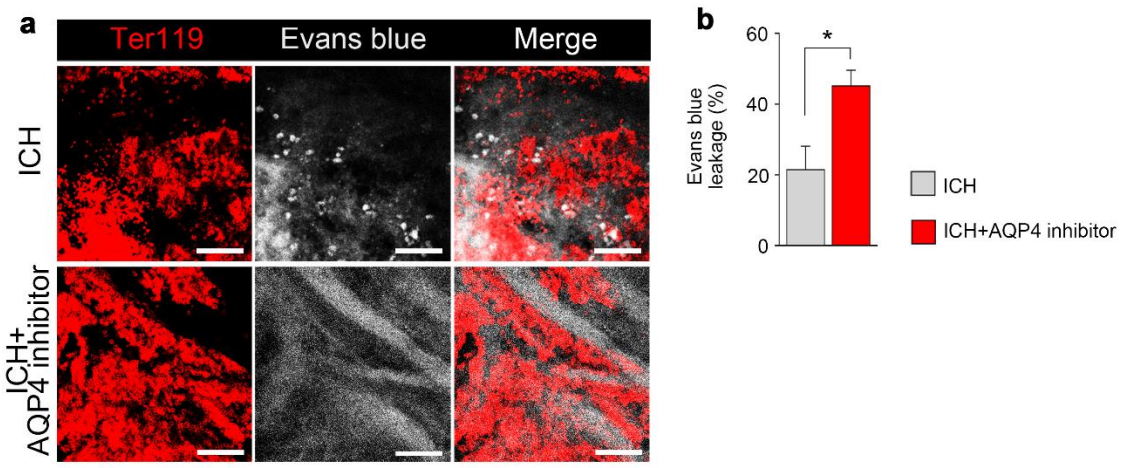

Figure 9. Increase of vascular permeability by AQP4 inhibitor administration.

(a) Immunofluorescence staining of Ter119+ red blood cells and Evans blue leakage (magnification x20). (b) Quantification of evans blue leakage in confocal microscopy of perihematomal edema. Data are mean ±SD. *p<0.05

3.2 Hemorrhage-derived reactive oxygen species (ROS) downregulates AQP4 expression in astrocytes

Our antibody-based protein array showed that AQP4 expression was significantly decreased in the PHE region, and we also observed that PHE was aggravated in $AQP4^{-/-}$ mice. These results suggest that some factors in PHE may reduce AQP4 expression. We thus tested whether hemorrhage-derived products (i.e., iron, urokinase, thrombin, and reactive oxygen species [ROS]) down-regulate the AQP4 expression *in vitro* (fig. 10a,10b). We found that ROS generated by intracerebral hemorrhage significantly reduced the AQP4 expression in the PHE. Therefore, we performed a co-culture of astrocytes and endothelial cells to confirm the role of ROS in regulating AQP4 expression in astrocytes (Fig. 11a). AQP4 expression was significantly reduced upon treatment with H_2O_2, which was effectively negated by co-treatment with N-acetylcysteine (NAC), a potent ROS scavenger (Fig. 12,13).

We also found that mice with intracerebral hemorrhage showed prominent activation of astrocytes (i.e., increased S100-beta expression, a higher number of dendrites) in their PHE region, which was also effectively negated upon co-treatment with NAC (Fig.14,15). In the PHE regions, the AQP4 expression reduction was accompanied by a significant elimination of astrocytes coverage on the blood vessels (Fig. 16a). Interestingly, the ROS expression site coincidently overlapped with the PHE region (Fig. 17a) and the region with reduced AQP4 expression. In this area, astrocyte coverages were eliminated from blood vessels. Still, they were effectively restored by ROS scavenger treatment (Fig. 18a), thus showing that ROS regulates AQP4 expression and astrocyte coverage on the blood vessels in the PHE. We then performed microdissection of the PHE region to identify the source of ROS production and found that the majority of ROS was produced by hemorrhage-derived products, astrocytes, and neurons (Fig.19,20,21). Our results collectively indicate that hemorrhage-derived ROS is a microenvironmental regulator of AQP4 expression and astrocyte coverage in PHE.

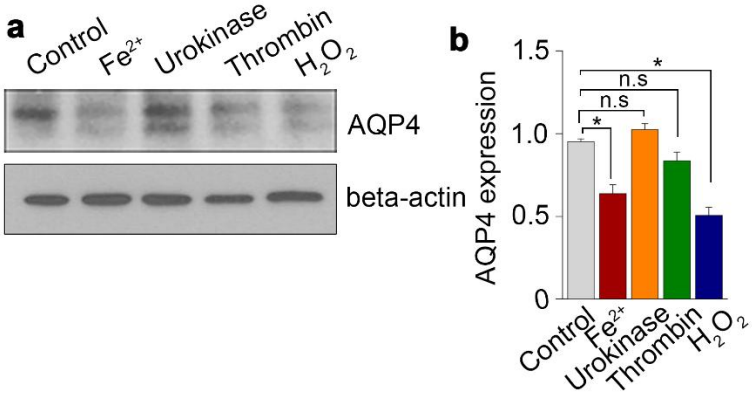

Figure 10. Decrease in AQP4 expression of astrocyte upon exposure to oxidative stress agents.

(a,b) Western blot analysis of AQP4 in astrocytes treated with indicated chemicals. The quantification graph is shown on the right (b). Data are mean±SD. *$p<0.05$.

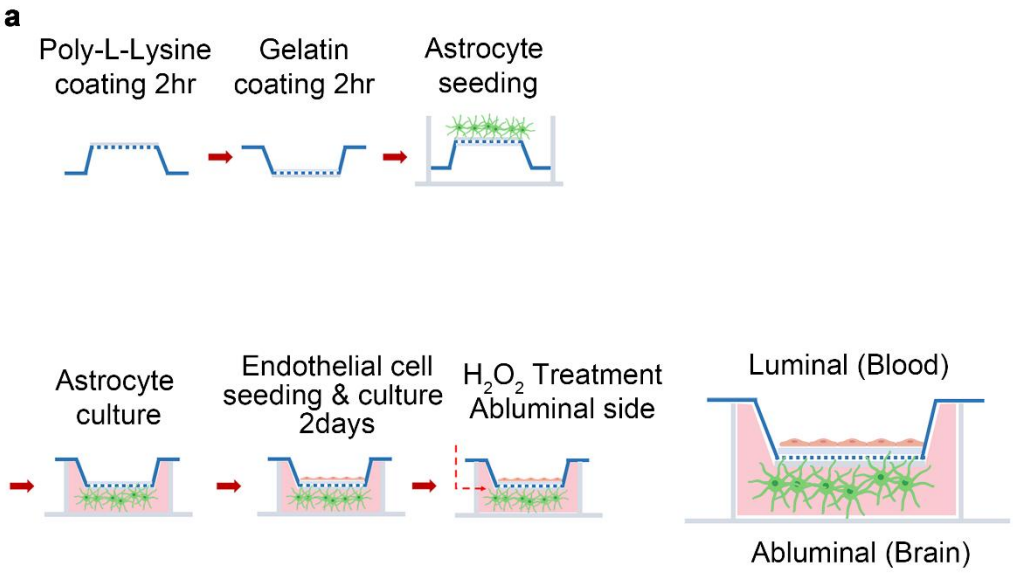

Figure 11. Illustration of the in vitro co-culture system of astrocyte and endothelial cells.

Human astrocyte seeded on poly-l-lysine-coated trans-well and were allowed to adhere overnight. After 2days, Endothelial cell seeded on gelatin-coated trans-well insert. After 2days, hydrogen peroxide treated on the abluminal side.

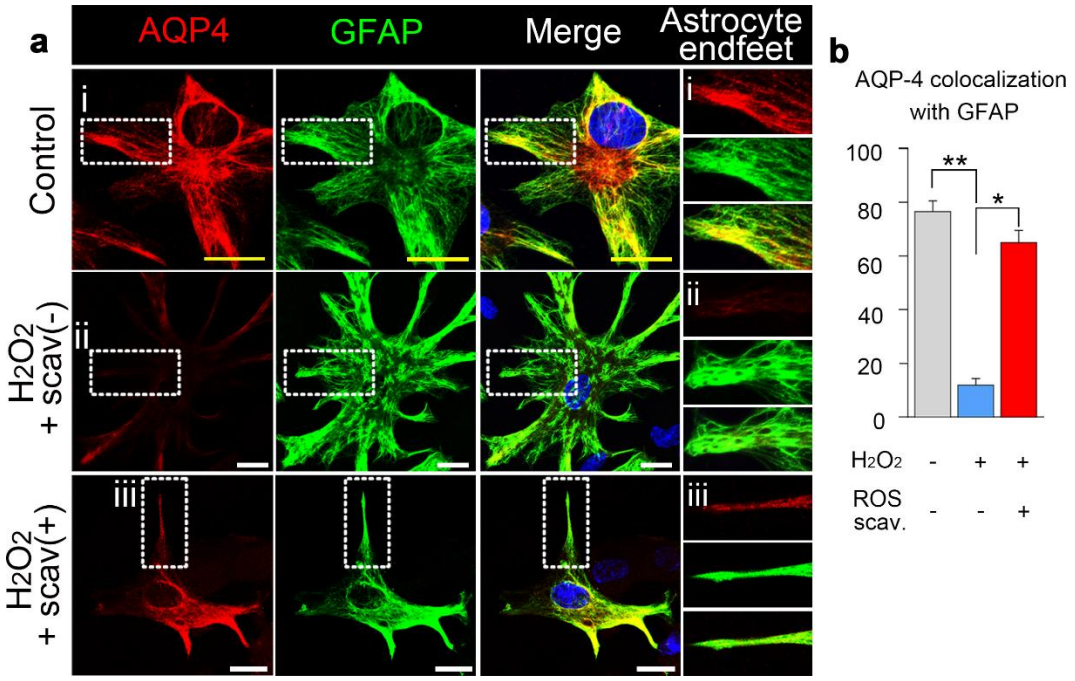

Figure 12. Morphological changes of astrocyte after oxidative stress.

(a,b) Representative confocal images of AQP4 in the astrocyte end-feet under treatment with hydrogen peroxide (H_2O_2) with or without ROS scavenger. Data are mean±SD. *$p<0.05$, **$p<0.01$.

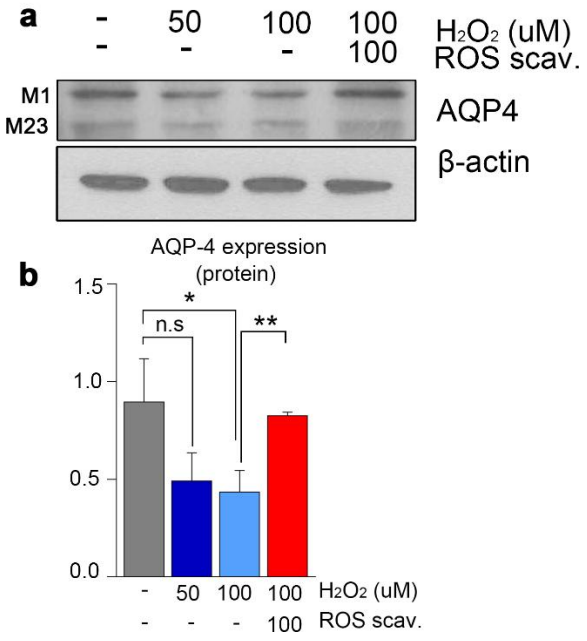

Figure 13. Increase of AQP4 protein expression after ROS scavenger treatment.

(a,b) Expression levels of AQP4 in astrocytes in the co-culture under treatment with H_2O_2 with or without ROS scavenger in indicated concentrations. Data are mean±SD. *p<0.05, **p<0.01.

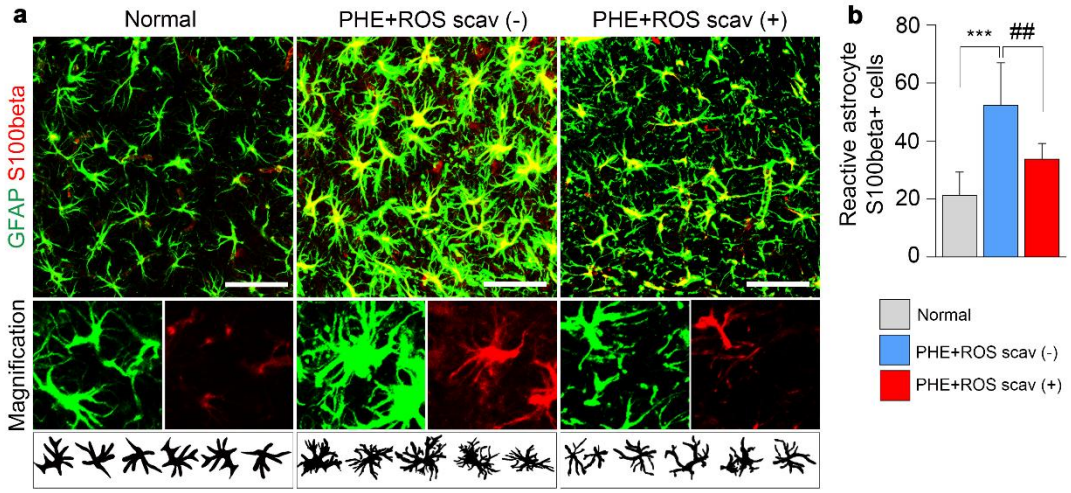

Figure 14. Morphological conversion of reactive astrocyte after perihematomal edema.

(a.b) Confocal images show GFAP+ astrocytes and S100beta+ reactive astrocyte in the normal brain region and PHE areas in mice treated with or without ROS scavenger. Schematic drawings of the astrocyte coverage and dendrites are shown in the lower panels (magnification x20). Data are mean±SD. ***$p<0.001$, ##$p<0.01$.

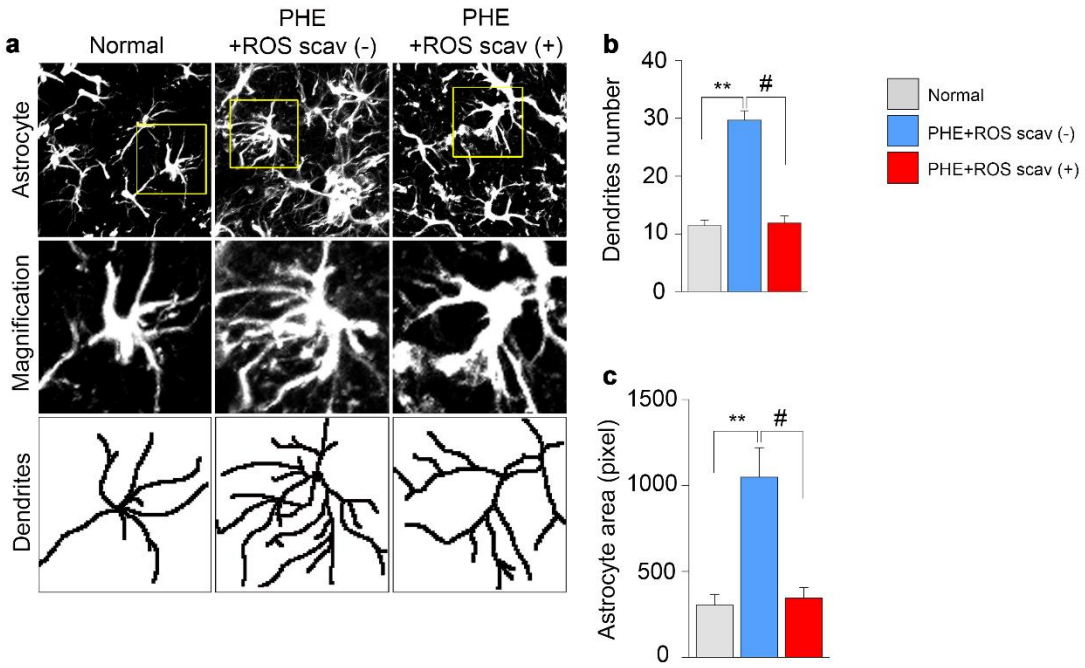

Figure 15. Morphological changes in reactive astrocytes.

(a,b,c) Comparisons of the number of reactive astrocytes (S100beta + cells), number of dendrites per cell, and astrocyte coverage in the normal brain region and PHE areas in mice treated with or without ROS scavenger. Data are mean±SD. **p<0.01, #p<0.05.

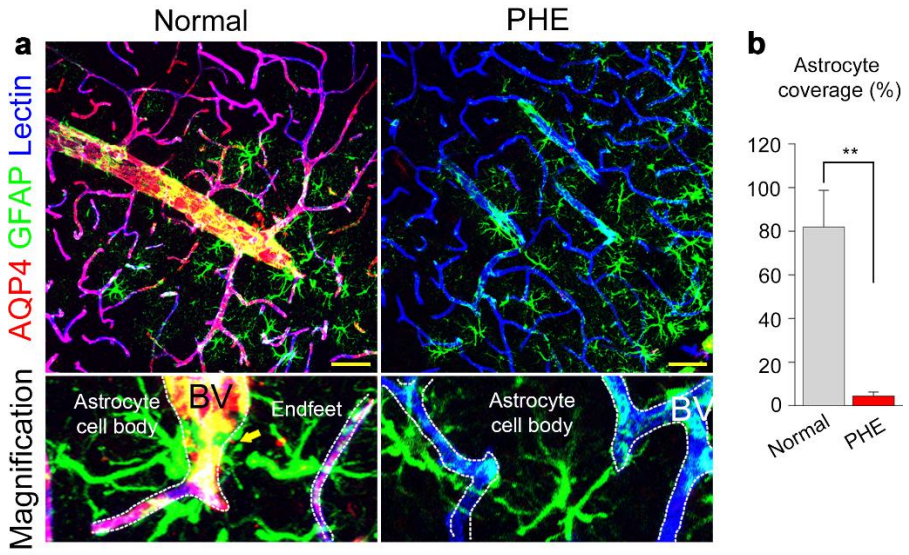

Figure 16. Astrocyte coverage surrounding the vessels in perihematomal region.

(a,b) Representative confocal images showing AQP4 expression in the astrocyte-foot process in normal tissue and PHE tissue (magnification x20). Data are mean±SD. *p<0.05.

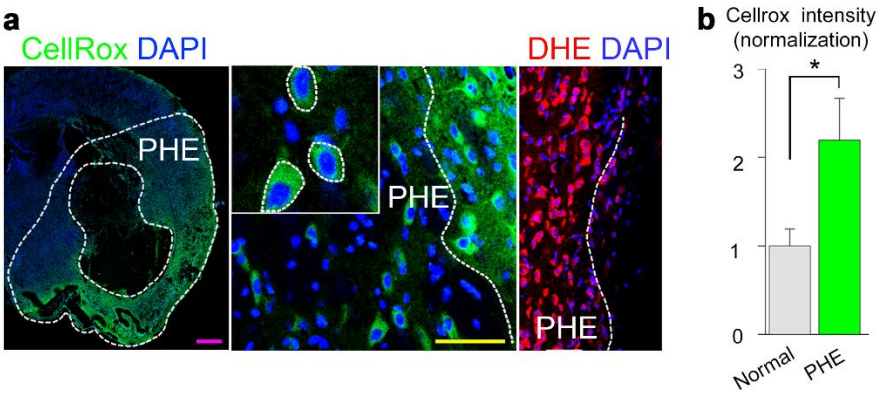

Figure 17. Detection of ROS production by CellRox and DHE fluorescence.

(a,b) Representative confocal images showing ROS expression (Cellrox,DHE) in the PHE area (magnification x20). Data are mean±SD. *$p<0.05$.

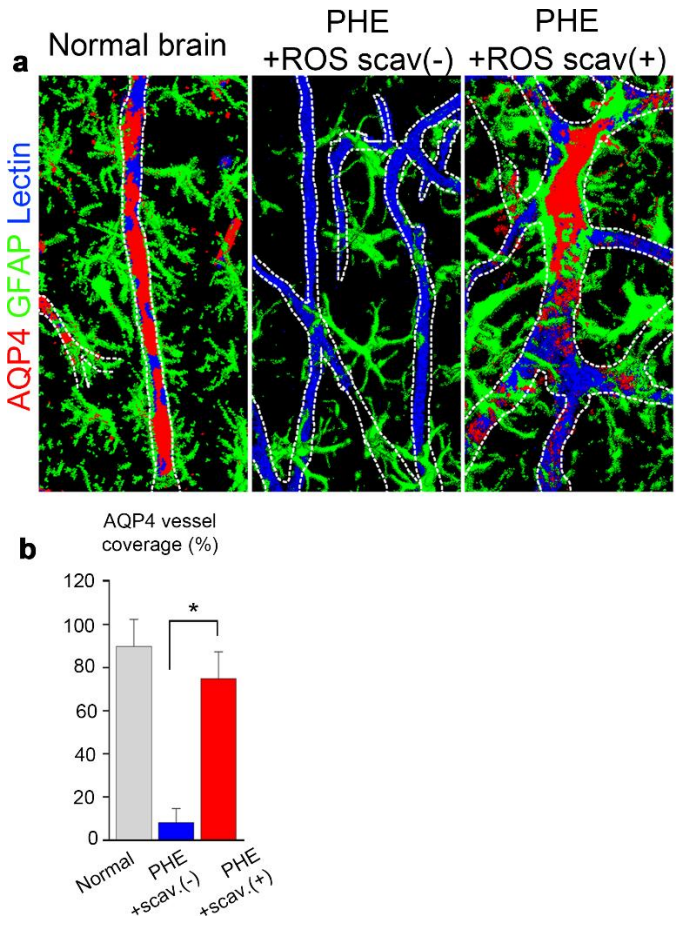

Figure 18. Recovery of astrocyte coverage after ROS scavenger treatment.

(a,b) Maximum intensity projection of brain vasculature after intracerebral hemorrhage. Data are mean±SD. *$p<0.05$.

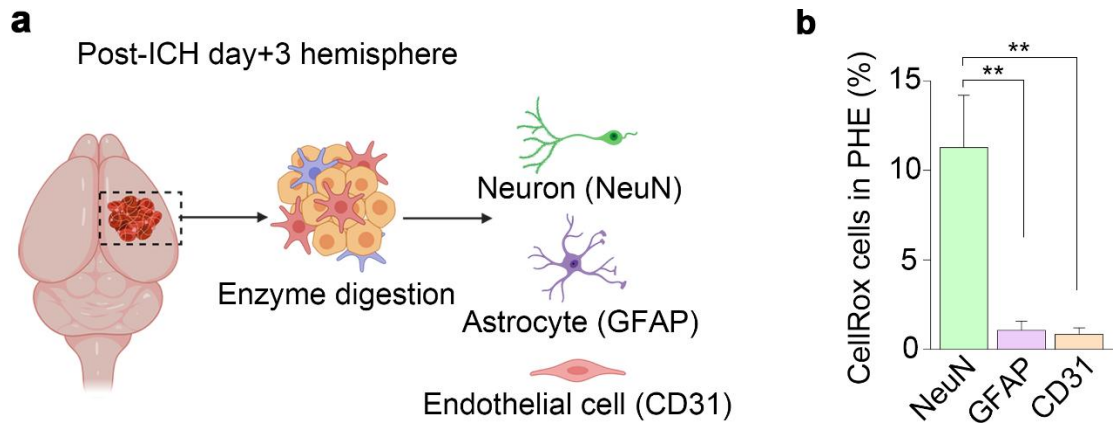

Figure 19. Generation of ROS by hematoma in neuron and astrocyte.

(a) Illustration of single-cell isolation after microdissection of the PHE area. (b) FACS data showing the source of ROS in the PHE area. Data are mean±SD. **p<0.01.

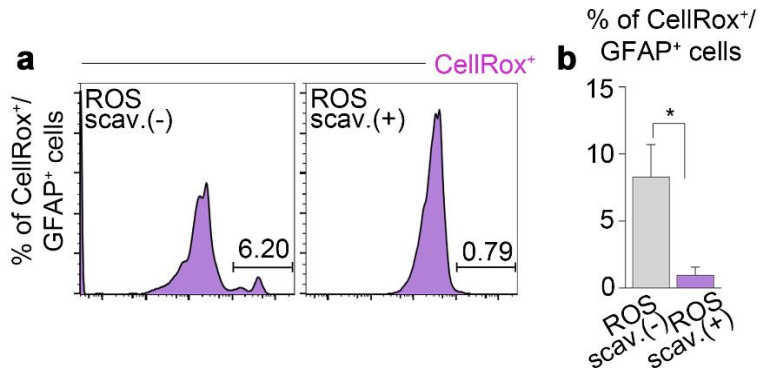

Figure 20. Estimation of astrocytic cellular ROS levels of perihematomal region.

(a,b) Flow cytometry analysis showing the proportion of astrocyte producing ROS (Cellrox+) with or without ROS scavenger. Data are mean±SD. *p<0.05.

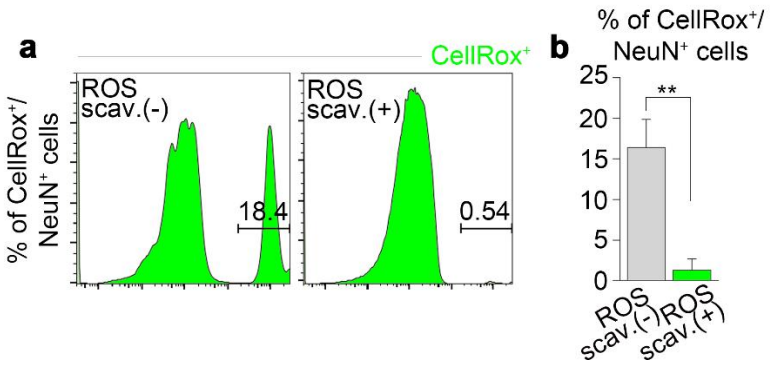

Figure 21. Estimation of neuronal cellular ROS levels of perihematomal region.

(a,b) Flow cytometry analysis showing the proportion of neuron producing ROS (Cellrox+) with or without ROS scavenger. Data are mean±SD. **p<0.01.

3.3 ROS scavenger and AQP4 enhancer alleviate perihematomal edema by improving blood-brain barrier integrity

We then investigated whether treatment with ROS scavengers, NAC, or Trolox can protect against the effects of intracerebral hemorrhage, reduce PHE, and restore the AQP4 expression. We also tested whether treatment with BQ-788, which enhances the AQP4 expression by antagonizing the endothelin B receptor (ETbR) [31], can also produce analogous effects with ROS scavengers. Each drug was administered every other day for two weeks after the hemorrhage induction (Fig. 22). Both ROS scavengers and BQ-788 effectively inhibited PHE formation (Fig. 23a) and BBB leakage (Fig. 24). Moreover, treatment with an ROS scavenger or an AQP enhancer resulted in improved survival rates (Fig. 23b). Similar to the result in $AQP4^{-/-}$ mice, ROS scavengers and AQP4 enhancer did not induce significant differences in the hematoma size (Fig. 23c) after hemorrhage induction but led to substantial reductions in the PHE extent (Fig. 23d) and EED corrected by the amount of hemorrhage (Fig. 23e). In addition, NAC treatment alleviated the PHE in AQP4-/- mice with cerebral hemorrhage (Fig. 25 a,d,e) and improved their survival rates (Fig. 25b).

The changes in the BBB components were examined to reveal the cellular mechanism of PHE prevention by ROS scavenger and AQP4 enhancer. Both the ROS scavenger and the AQP4 enhancer significantly restored the expression levels of PDGFR-beta (Fig. 26a,b), VE-cadherin (Fig. 27a,b), and laminin (Fig. 29a,b), AQP4 (Fig. 28a,b), and astrocyte coverage (Fig. 31a,b). Notably, the ROS scavenger and the AQP4 enhancer showed comparable beneficial effects on the BBB microstructures. The expression of tight junction protein Claudin-5 was also increased upon treatment with an ROS scavenger or an AQP4 enhancer (Fig. 30a,b). These results collectively indicate that ROS is responsible for the pathophysiology of the PHE formation through the BBB disruption due to reduced AQP4 expression in astrocytes. AQP4 enhancement is effective in restoring the BBB's structural integrity. Fig. 35 illustrates our findings on the structural changes

in the BBB following intracerebral hemorrhage.

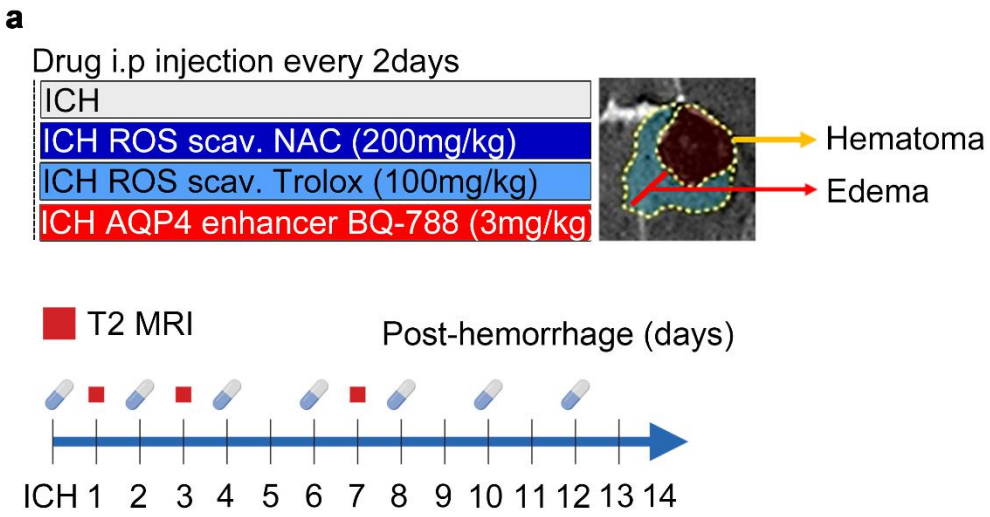

Figure 22. Experimental scheme of intracerebral hemorrhage model.

(a) Dosing schedule of the ROS scavengers (NAC, Trolox) and the AQP4 enhancer (BQ-788) and the MRI schedule

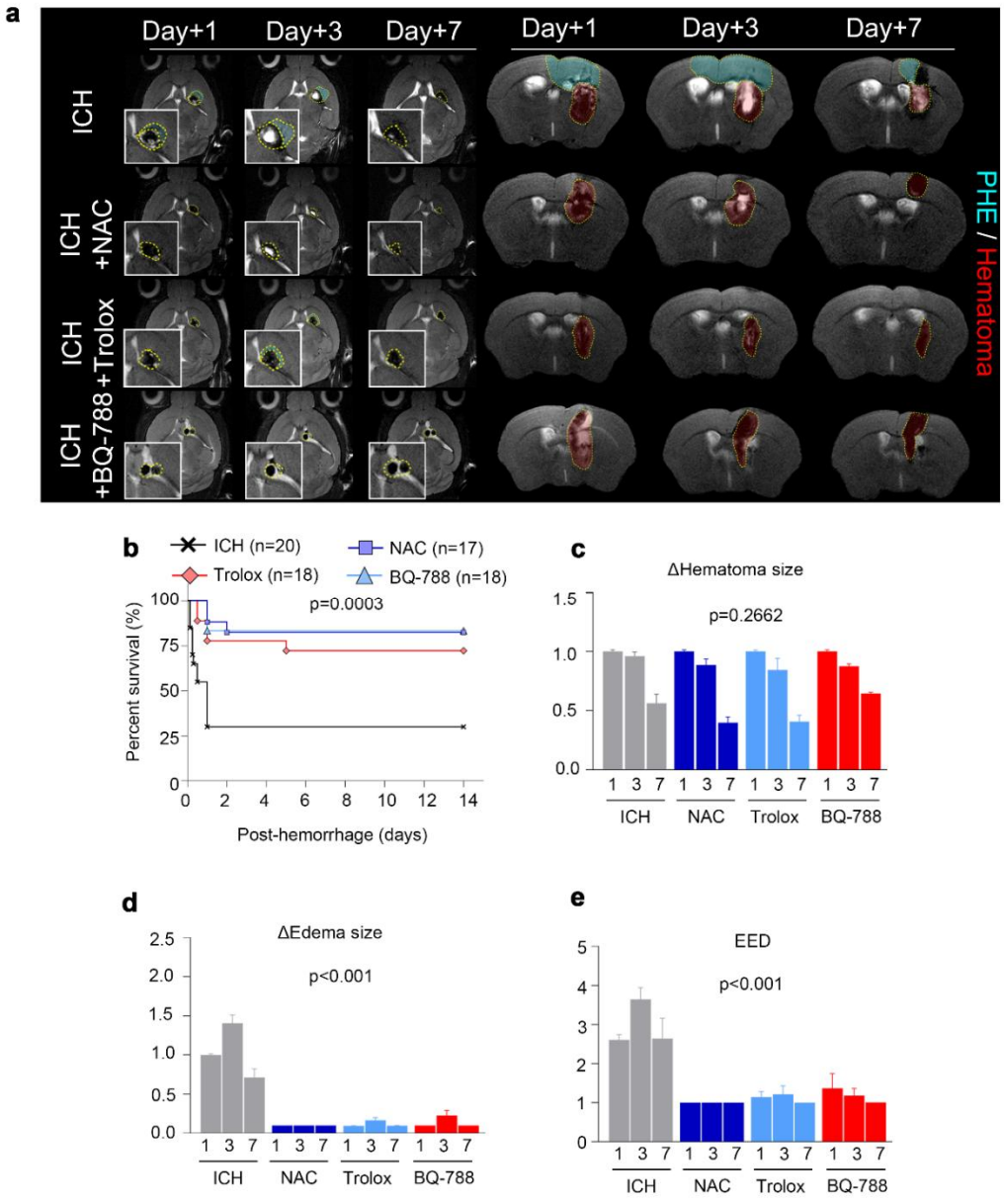

Figure 23. Reduction of edema during the ROS scavenger and AQP4 enhancer administration.

(a) T2-weighted MRI images acquired at 1,3, and 7 days after intracerebral hemorrhage showing the areas of PHE and hematoma. (b) Survival curves of the mice after intracerebral hemorrhage. (c,d,e) Changes in the size of hematoma, edema, and EED in the PHE region at 1,3 and 7days after intracerebral hemorrhage in mice. Data are mean ±SD.

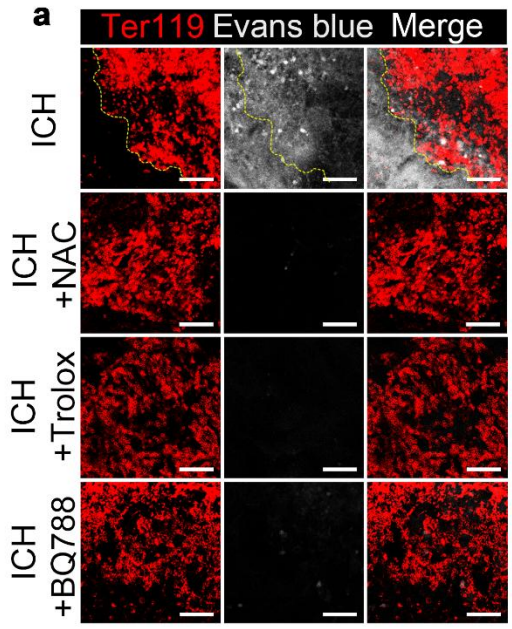

Figure 24. Reduction of vascular leakage by ROS scavenger and AQP4 enhancer.

(a) Evans blue leakage assay demonstrating the improving leakages by ROS scavenger (NAC, Trolox) and AQP4 enhancer (BQ-788) (magnification x20).

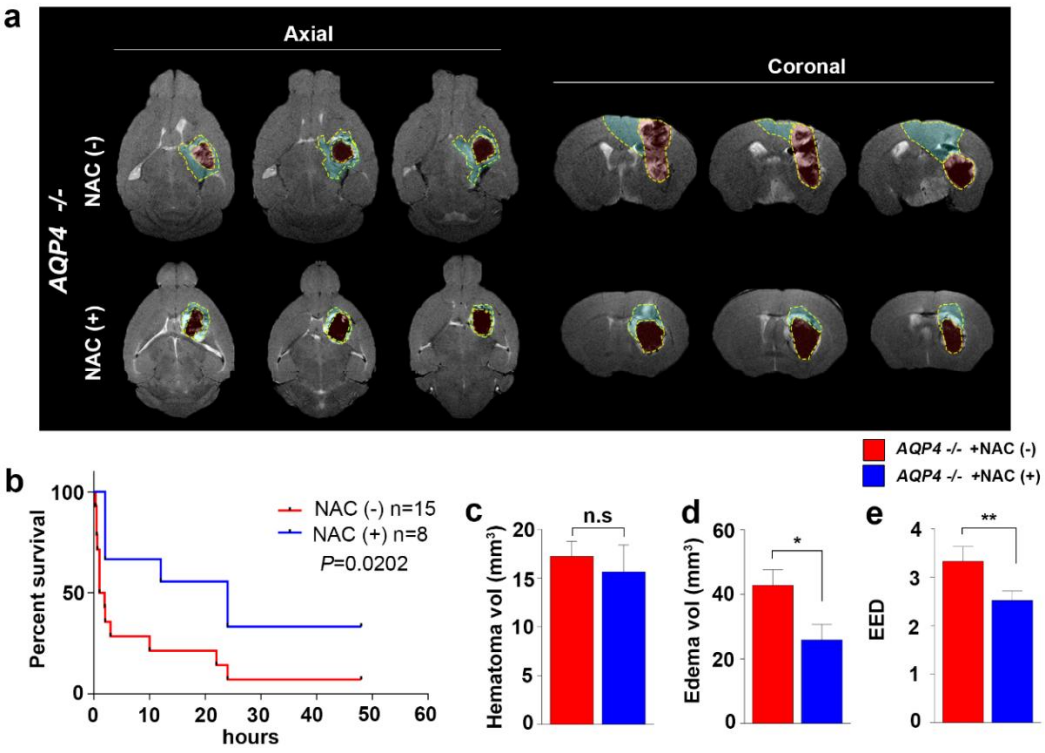

Figure 25. Effectiveness of edema resolution in AQP4 $^{-/-}$ group by ROS scavenger.

(a) MR images showing the PHE and hematoma in AQP4 $^{-/-}$ mice (untreated and treated with ROS scavenger). (b) Survival curves of AQP4 $^{-/-}$ mice after intracerebral hemorrhage. (c,d,e) Hematoma volumes, edema volumes, and EED of AQP4 $^{-/-}$ mice after intracerebral hemorrhage. Data are mean±SD. *p<0.05, **p<0.01.

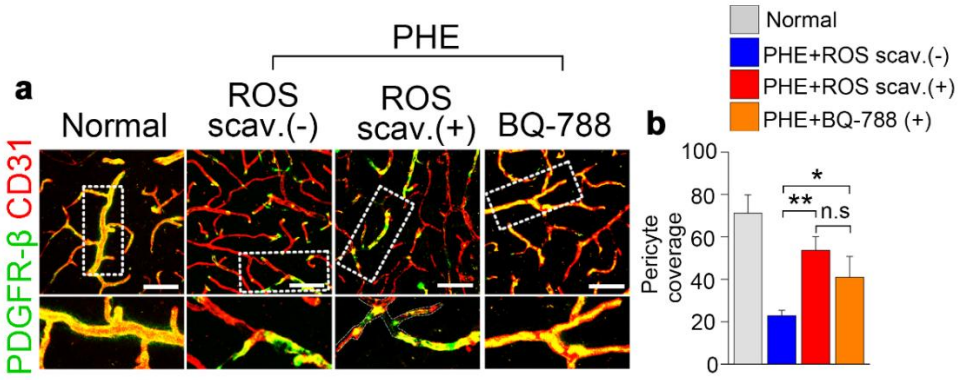

Figure 26. Analysis of pericyte of the BBB components in intracerebral hemorrhage.

(a,b) Confocal microscopy of the PDGFR-beta (pericyte) and CD31 (vessel) in the normal area and PHE area under the indicated conditions. Scale bar 50μm.Data are mean±SD. *p<0.05, **p<0.01.

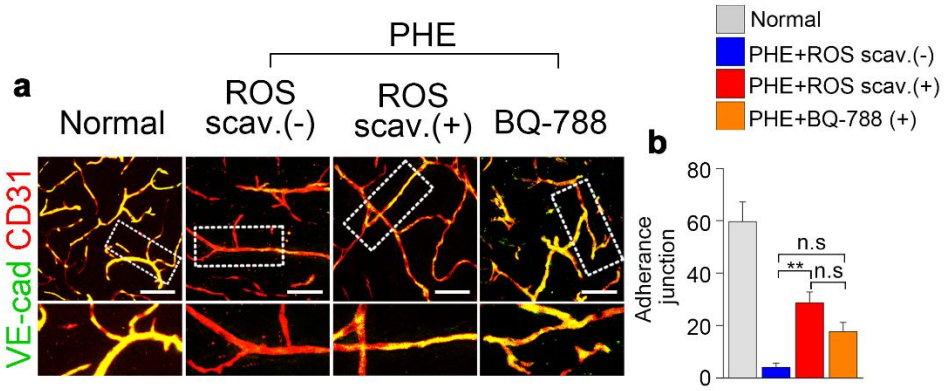

Figure 27. Analysis of adherence junction of the BBB components in intracerebral hemorrhage.

(a,b) Confocal microscopy of the VE-cadherin (junction) and CD31 (vessel) in the normal area and PHE area under the indicated conditions. Scale bar 50μm.Data are mean±SD. *p<0.05, **p<0.01.

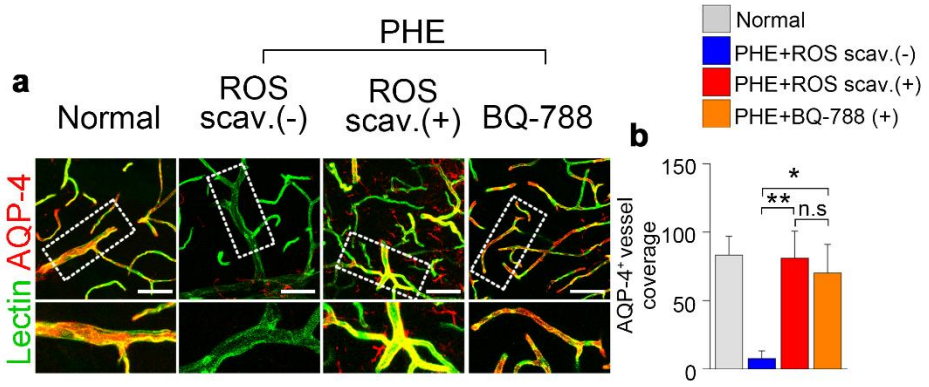

Figure 28. Analysis of astrocyte end-feet process of the BBB components in intracerebral hemorrhage.

(a,b) Confocal microscopy of the AQP-4 (astrocyte end feet) and Lectin (vessel) in the normal area and PHE area under the indicated conditions. Scale bar 50μm.Data are mean±SD. *p<0.05, **p<0.01.

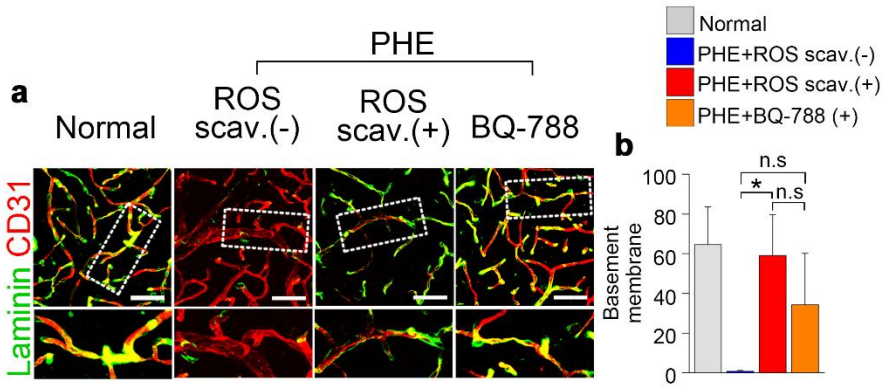

Figure 29. Analysis of basement membrane of the BBB components in intracerebral hemorrhage.

(a,b) Confocal microscopy of the Laminin (basement membrane) and CD31 (vessel) in the normal area and PHE area under the indicated conditions. Scale bar 50μm.Data are mean±SD. *$p<0.05$.

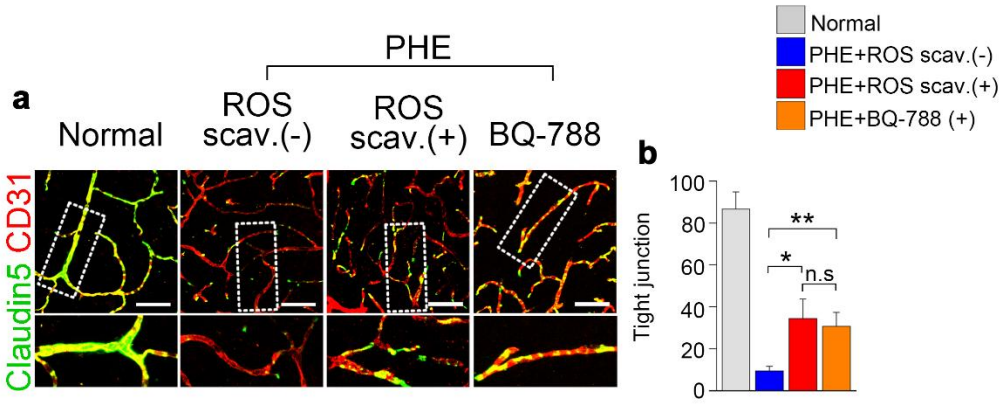

Figure 30. Analysis of tight junction of the BBB components in intracerebral hemorrhage.

(a,b) Confocal microscopy of the Claudin-5 (tight junction) and CD31 (vessel) in the normal area and PHE area under the indicated conditions. Scale bar 50μm.Data are mean±SD. *p<0.05.

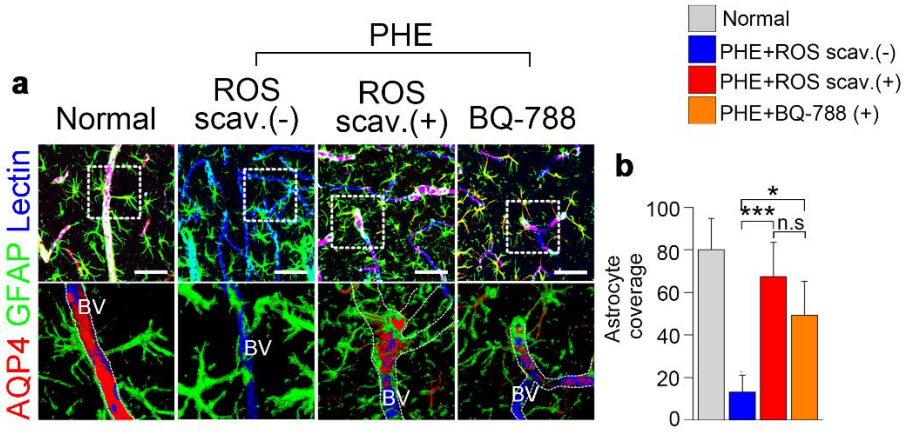

Figure 31. Analysis of astrocyte coverage and end-feet process of the BBB components in intracerebral hemorrhage.

(a,b) Confocal microscopy of the AQP4 (end-feet) GFAP (astrocyte) and Lectin (vessel) in the normal area and PHE area under the indicated conditions. Scale bar 50μm. Data are mean±SD. *p<0.05.

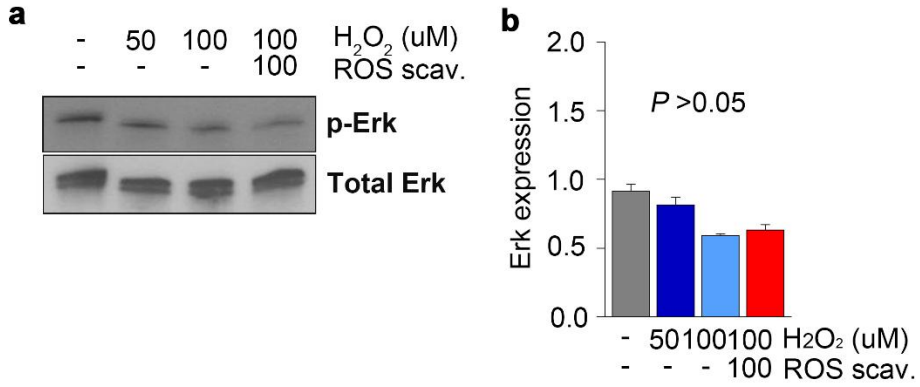

Figure 32. Analysis of Erk pathway in astrocytes after oxidative stress.

(a,b) Astrocytes were treated with the indicated concentrations of H_2O_2 to induce ROS stress. ROS stress did not significantly affect the expression levels of common proliferative signal molecules. Data are mean±SD.

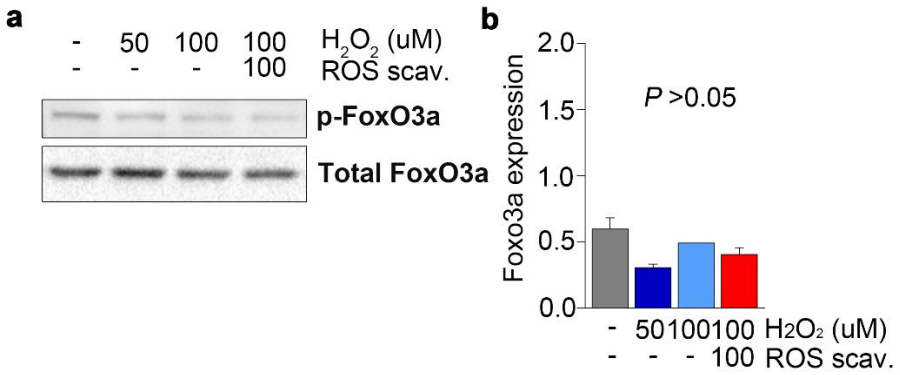

Figure 33. Analysis of FoxO3a pathway in astrocyte after oxidative stress.

(a,b) Astrocytes were treated with the indicated concentrations of H_2O_2 to induce ROS stress. ROS stress did not significantly affect the expression levels of common proliferative signal molecules. Data are mean±SD.

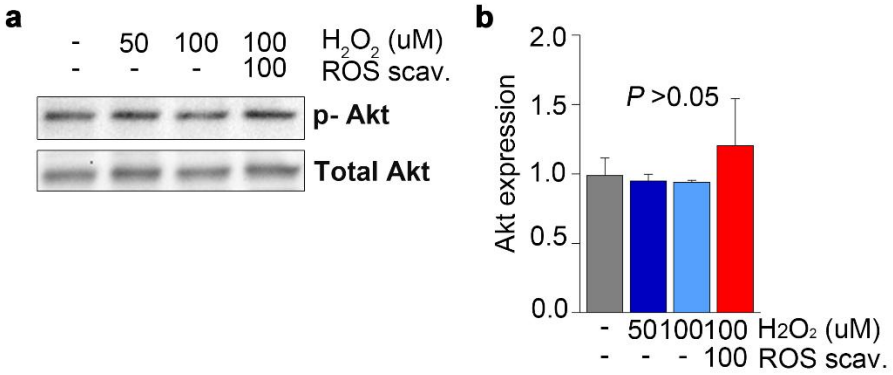

Figure 34. Analysis of Akt pathway in astrocytes after oxidative stress.

(a,b) Astrocytes were treated with the indicated concentrations of H_2O_2 to induce ROS stress. ROS stress did not significantly affect the expression levels of common proliferative signal molecules. Data are mean±SD.

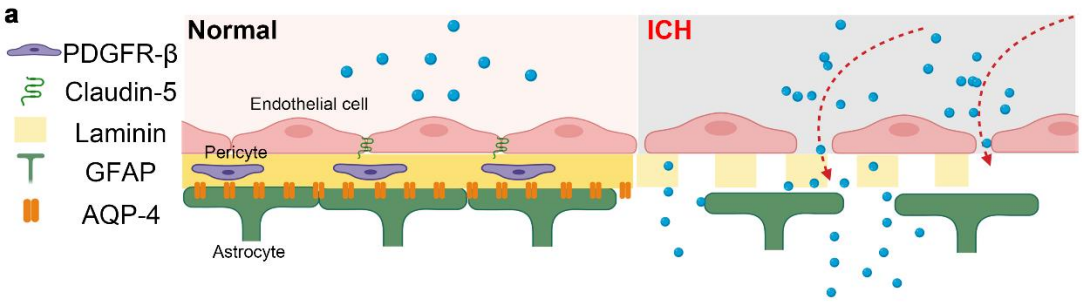

Figure 35. Microstructure of the BBB after intracerebral hemorrhage.

(a) In the steady state, the BBB is a structurally stable complex formed by the pericyte (PDGFR-beta), Tight junction (claudin-5), basement membrane (laminin), and end-feet of the astrocyte process. However, after intracerebral hemorrhage, PHE occurs due to the disruption of the BBB structure. Among the BBB structures of microvessels, pericyte, laminin, VE-cadherin, and astrocyte coverage are decreased in PHE.

Discussion

Most patients with intracerebral hemorrhage develop varying degrees of PHE, which adversely affects the clinical course by increasing intracranial pressure [4, 32, 33]. For this reason, the resolution of PHE is vital for reducing morbidity and mortality. However, there are no direct treatments for PHE. The indirect treatment of removing the excessive accumulation of water from the brain parenchyma by inducing osmotic diuresis has shown unsatisfactory results [1]. Therefore, our results on the use of ROS scavenger and AQP4 enhancer to reduce the PHE volume in patients with intracerebral hemorrhage seem promising.

Early PHE is mainly caused by the Na^+-K^+ pump dysfunction, which is due to insufficient oxygen and energy supply by the microvascular shutdown in intracerebral hemorrhage [33]. The resulting disruption of the ion gradient between cell membranes leads to cytotoxic edema in the brain parenchyma. The brain is a highly active and plastic organ with significant energetic needs, and intracerebral hemorrhage could lead to disturbances in the energetic balance or glia-neuron metabolic interaction. Under physiological conditions, the major energy source for the brain is glucose [34]. Although neurons require a high amount of energy, they possess a minimal energy reserve that can satisfy only a small portion of the energy demand. Therefore, neurons are dependent on the supply of energy substrates such as lactate from the blood through the blood-brain barrier (BBB) and astrocytes (i.e., astrocyte-neuron lactate shuttle [ANLS]). BBB and astrocytes that are damaged under the PHE condition cannot properly supply energy substrates to neurons, leading to the aggravation of neuronal death-associated edema [35-40].

Conversely, as shown in our animal model of intracerebral hemorrhage, delayed PHE can occur due to excessive water leakage through the disrupted BBB or defects in removing excessive water through water channels [41]. In clinical practice, delayed PHE resulting from disruption of the BBB is often more problematic than cytotoxic edema that occurs immediately after hemorrhage

[42]. The BBB disruption in PHE is due to inflammatory response, excitotoxicity, and increased free radicals; particularly, the increases in interleukin-1,2, and 6 [43] as well as activated MMP 3,9 cascade [44] in astrocytes by hemorrhage-induced inflammation result in tight junction damage [45]. As a result, toxic substances such as inflammatory cells [46], urokinase [47], thrombin [48], and haptoglobin [49] in the bloodstream can leak through the disrupted BBB and potentiate delayed PHE along with additional local inflammation. Subsequent inflammatory reactions that occur in the PHE activate the MMP cascade and increase the production of reactive oxygen-nitrogen species ($^{\bullet}$O2-, H_2O_2, $^{\bullet}$OH-, $^{\bullet}$NO, ONOO-) [50] and glutamate from glial cells such as activated microglia and astrocytes [51].

In our current study, the AQP4 expression on BBB's astrocyte coverage was reduced by ROS generated in intracerebral hemorrhage. Because the astrocyte coverage functions as the outer skeleton in maintaining overall BBB integrity, the decrease of AQP4 expression on astrocytes resulted in disrupting the BBB microstructures, including pericyte, basement membrane, and astrocyte coverage. As a result, leakage through BBB occurred rapidly, and PHE developed in the early stage of intracerebral hemorrhage.

In eukaryotic cells, ROS are generally produced in the reactions catalyzed by NAD(P)H oxidase and other specialized oxidases as well as the by-product of redox reactions. Intracellular ROS synthesis is regulated by various hormones, cytokines, and growth factors; however, in intracerebral hemorrhage, a large amount of extracellular ROS is generated from hemoglobin and ferrous end products[52, 53]. An increase in the ROS levels above a certain threshold is accompanied by detrimental processes for cell survival, such as lipid peroxidation and oxidative modification of proteins and nucleic acids. In our additional experiment, we found that ROS generated in intracerebral hemorrhage did not significantly alter the expression levels of cell signaling molecules involved in the survival and proliferation of astrocytes such as Erk, Akt, and FOXO3a (Supplementary Fig.4). Thus, ROS is not likely to have affected the expression of AQP4 through the proliferative signaling pathway in astrocytes. However, some studies have shown that

hypothermia, calcium receptor, and calmodulin-mediated mechanisms affect the surface trafficking of AQP4. In addition, ROS may also affect the expression level of AQP4 or its surface localization [54, 55]. Considering our *in vitro* experiments about the ROS-mediated AQP4 expression reduction in astrocytes, ROS seems to decrease the AQP4 expression through cellular mechanisms other than the canonical proliferative signaling cascade or post-translational modification.

The current treatment modalities for PHE are mostly indirect methods in which the excess water in the brain parenchyma is removed by administering hyper-osmotic agents such as mannitol and hypertonic saline [2]. However, the indirect methods have limited effects and often entail adverse effects such as rebound edema and renal toxicity. There are some direct strategies for alleviating PHE, which involve increasing the expression or function of the defective components of the BBB. A representative direct method is the administration of HMG-CoA reductase (e.g., atorvastatin). They showed pleiotropic effects in the tandem proliferation of pericytes, thereby improving the BBB's pericytes coverage, followed by reducing PHE's degree [56-58]. However, such direct methods seem to be primarily effective in preventing PHE development in patients taking the drug prior to the intracerebral hemorrhage, rather than alleviating the PHE after it has formed. Other direct methods include glibenclamide, which suppresses the functions of MMP-9 that are increased in intracerebral hemorrhage and induces local inflammation. Still, glibenclamide effects are yet to be fully supported through clinical trials [59]. In this aspect, our study is notable in that it focused on astrocytes, which are relatively overlooked but comprise the largest proportion of cells in the brain. Specifically, we sought to improve the BBB coverage by astrocytes in alleviating PHE. We also found that enhancing the expression and function of AQP4 in astrocytes is an effective way to achieve this goal. AQP4 in the end-feet of astrocytes is advantageous as a clinical target because it maintains the BBB's structural integrity to suppress the development of the PHE and can actively clear existing PHE. Considering that there are no clinically proven methods for directly alleviating PHE, our results on the potential therapeutic

effect of AQP4 modulation seem promising.

AQPs have been validated as an important drug target, but no single drug has been approved to successfully target them. Although some potential AQP modulators have been identified, there are still challenges associated with developing better modulators such as the druggability of the target and the suitability of the assay methods used for identifying the modulators. Since AQP4 is also still an elusive drug target, it may be better to consider alternative routes to the traditional pore-blocking approach, such as gene transfer or an antibody targeting the function of AQP4 [60, 61]. In mice treated with TGN-020, the expression of AQP4 was lower than that in untreated control mice, followed by more prominent PHE formation and poorer survival outcomes. However, the AQP4 inhibition experiment is limited in that the reversible effect of AQP4 targeting could not be assessed. Therefore, the cell surface expression of AQP4 should be evaluated through *in vitro* experiments to assess the reversibility according to the tonicity of targeting agents [20, 62].

In this study, TGN-020 was found to inhibit AQP4 based on Xenopus laevis oocyte swelling assays. However, there are concerns that the inhibitory action of TGN-020 is not readily reproducible in other assays, and that TGN-020 has effects on brain water transport independent of AQP4, thus confounding the interpretation of *in vivo* studies. In addition, the off-target effects of TGN-020 are largely unknown. Therefore, the action of TGN-020 on AQP4 is somewhat ambiguous and requires careful interpretation. Although the deterioration of PHE by TGN-020 might be due to its off-target effects, the *in vivo* role of TGN-020 in the inhibition of AQP4 was clearly shown as the PHE of mice treated with TGN-020 was more severe than that in control mice. The mode and mechanism of AQP4 inhibition by TGN-020 should be further identified in future studies [63].

Treatment with ROS scavengers restored the expression of AQP4 *in vivo* and *in vitro* and improved the BBB's overall integrity; notably, treatment with AQP4 enhancer produced similar

beneficial effects, indicating the potential usefulness of AQP4 as a clinical target in ROS-mediated neurological diseases. The ROS scavenger has been known to reduce the edema by modulating local inflammation; however, our results collectively indicate that the ROS scavenger could reduce the PHE by restoring the AQP4 expression and subsequently improving the BBB integrity. Our culture system is a 2D culture system using a transwell. Therefore, there might be some limitations in evaluating the expression of AQP4, which shows a polarized pattern in the astrocyte end-feet. Through 3D culture, the expression of AQP4 in the astrocyte end-feet can be determined more accurately. The 3D-perfused system provides physiologically relevant insight and is more beneficial for evaluating the underlying signaling mechanisms and functions. In this regard, future studies need to utilize real-time monitoring of AQP4 expression using a 3D-self-organized model or a microvessel-on-a-chip platform [64, 65].

Importantly, we found that the treatment of mice with intracerebral hemorrhage with ROS scavenger significantly reduced PHE volume, which is likely via the restoration of the water channel AQP4 that promotes the clearance of excessive water buildup. Conversely, the experiments using $AQP4^{-/-}$ mice and an AQP4 enhancer suggested that AQP4 also has a pivotal role in suppressing the PHE formation by maintaining BBB's structural integrity. Thus, our results collectively suggest that AQP4 may be a useful clinical target for treating the PHE and its prevention. Although some potential AQP modulators have been identified, there are challenges associated with developing better modulators such as the druggability of the target and the suitability of the assay methods used for identifying potential modulators. Therefore, various advanced attempts are needed to develop new drugs targeting AQPs. In addition, screening of extensive libraries with efficient high-throughput screening (HTS) has become a vital process in drug discovery. HTS can screen thousands of compounds per day; however, if fewer compounds could be screened without compromising the probability of success, the cost and time would be largely reduced. Finally, recent advances in computer-aided design, in silico libraries, and molecular docking software combined with the upscaling of cell-based platforms have evolved to

improve screening efficiency with higher predictability and clinical applicability [60, 66, 67].

References

1. Qureshi, A.I., A.D. Mendelow, and D.F. Hanley, *Intracerebral haemorrhage.* Lancet, 2009. **373**(9675): p. 1632-44.
2. Qureshi, A.I., et al., *Spontaneous intracerebral hemorrhage.* N Engl J Med, 2001. **344**(19): p. 1450-60.
3. Stokum, J.A., V. Gerzanich, and J.M. Simard, *Molecular pathophysiology of cerebral edema.* J Cereb Blood Flow Metab, 2016. **36**(3): p. 513-38.
4. Simard, J.M., et al., *Brain oedema in focal ischaemia: molecular pathophysiology and theoretical implications.* Lancet Neurol, 2007. **6**(3): p. 258-68.
5. Armulik, A., et al., *Pericytes regulate the blood-brain barrier.* Nature, 2010. **468**(7323): p. 557-61.
6. Bell, R.D., et al., *Pericytes control key neurovascular functions and neuronal phenotype in the adult brain and during brain aging.* Neuron, 2010. **68**(3): p. 409-27.
7. King, L.S., D. Kozono, and P. Agre, *From structure to disease: the evolving tale of aquaporin biology.* Nat Rev Mol Cell Biol, 2004. **5**(9): p. 687-98.
8. Day, R.E., et al., *Human aquaporins: regulators of transcellular water flow.* Biochim Biophys Acta, 2014. **1840**(5): p. 1492-506.
9. Haj-Yasein, N.N., et al., *Glial-conditional deletion of aquaporin-4 (Aqp4) reduces blood-brain water uptake and confers barrier function on perivascular astrocyte endfeet.* Proc Natl Acad Sci U S A, 2011. **108**(43): p. 17815-20.
10. Hara-Chikuma, M. and A.S. Verkman, *Physiological roles of glycerol-transporting aquaporins: the aquaglyceroporins.* Cell Mol Life Sci, 2006. **63**(12): p. 1386-92.
11. Kitchen, P., et al., *Beyond water homeostasis: Diverse functional roles of mammalian aquaporins.* Biochim Biophys Acta, 2015. **1850**(12): p. 2410-21.

12. Kitchen, P., et al., *Water channel pore size determines exclusion properties but not solute selectivity.* Sci Rep, 2019. **9**(1): p. 20369.

13. Tomassoni, D., V. Bramanti, and F. Amenta, *Expression of aquaporins 1 and 4 in the brain of spontaneously hypertensive rats.* Brain Res, 2010. **1325**: p. 155-63.

14. Xi, T., et al., *miR-27a-3p protects against blood-brain barrier disruption and brain injury after intracerebral hemorrhage by targeting endothelial aquaporin-11.* J Biol Chem, 2018. **293**(52): p. 20041-20050.

15. Papadopoulos, M.C. and A.S. Verkman, *Aquaporin water channels in the nervous system.* Nat Rev Neurosci, 2013. **14**(4): p. 265-77.

16. Tait, M.J., et al., *Water movements in the brain: role of aquaporins.* Trends Neurosci, 2008. **31**(1): p. 37-43.

17. Papadopoulos, M.C., et al., *Aquaporin-4 facilitates reabsorption of excess fluid in vasogenic brain edema.* Faseb j, 2004. **18**(11): p. 1291-3.

18. Thrane, A.S., et al., *Critical role of aquaporin-4 (AQP4) in astrocytic Ca2+ signaling events elicited by cerebral edema.* Proc Natl Acad Sci U S A, 2011. **108**(2): p. 846-51.

19. Yang, B., Z. Zador, and A.S. Verkman, *Glial cell aquaporin-4 overexpression in transgenic mice accelerates cytotoxic brain swelling.* J Biol Chem, 2008. **283**(22): p. 15280-6.

20. Kitchen, P., et al., *Targeting Aquaporin-4 Subcellular Localization to Treat Central Nervous System Edema.* Cell, 2020. **181**(4): p. 784-799.e19.

21. Sylvain, N.J., et al., *The effects of trifluoperazine on brain edema, aquaporin-4 expression and metabolic markers during the acute phase of stroke using photothrombotic mouse model.* Biochim Biophys Acta Biomembr, 2021. **1863**(5): p. 183573.

22. Rynkowski, M.A., et al., *A mouse model of intracerebral hemorrhage using autologous blood infusion.* Nat Protoc, 2008. **3**(1): p. 122-8.

23. Parry-Jones, A.R., et al., *Edema Extension Distance: Outcome Measure for Phase II Clinical Trials Targeting Edema After Intracerebral Hemorrhage.* Stroke, 2015. **46**(6): p. e137-40.

24. Parry-Jones, A.R., et al., *Edema Extension Distance.* Stroke, 2015. **46**(6): p. e137-e140.

25. Wu, T.Y., et al., *Natural History of Perihematomal Edema and Impact on Outcome After Intracerebral Hemorrhage.* Stroke, 2017. **48**(4): p. 873-879.

26. Karuppagounder, S.S., et al., *N-acetylcysteine targets 5 lipoxygenase-derived, toxic lipids and can synergize with prostaglandin E(2) to inhibit ferroptosis and improve outcomes following hemorrhagic stroke in mice.* Ann Neurol, 2018. **84**(6): p. 854-872.

27. Zille, M., et al., *Neuronal Death After Hemorrhagic Stroke In Vitro and In Vivo Shares Features of Ferroptosis and Necroptosis.* Stroke, 2017. **48**(4): p. 1033-1043.

28. Moldes, O., et al., *Neuroprotection afforded by antagonists of endothelin-1 receptors in experimental stroke.* Neuropharmacology, 2012. **63**(8): p. 1279-85.

29. Li, J., et al., *TGN-020 alleviates edema and inhibits astrocyte activation and glial scar formation after spinal cord compression injury in rats.* Life Sci, 2019. **222**: p. 148-157.

30. Helms, H.C., et al., *In vitro models of the blood-brain barrier: An overview of commonly used brain endothelial cell culture models and guidelines for their use.* J Cereb Blood Flow Metab, 2016. **36**(5): p. 862-90.

31. Kim, J.E., H.J. Ryu, and T.C. Kang, *Status epilepticus induces vasogenic edema via tumor necrosis factor-α/ endothelin-1-mediated two different pathways.* PLoS One, 2013. **8**(9): p. e74458.

32. Balami, J.S. and A.M. Buchan, *Complications of intracerebral haemorrhage.* Lancet Neurol, 2012. **11**(1): p. 101-18.

33. Urday, S., et al., *Targeting secondary injury in intracerebral haemorrhage--perihaematomal oedema.* Nat Rev Neurol, 2015. **11**(2): p. 111-22.

34. Dienel, G.A., *Brain lactate metabolism: the discoveries and the controversies.* J Cereb Blood Flow Metab, 2012. **32**(7): p. 1107-38.

35. Ebert, D., R.G. Haller, and M.E. Walton, *Energy contribution of octanoate to intact rat brain metabolism measured by 13C nuclear magnetic resonance spectroscopy.* J Neurosci, 2003. **23**(13): p. 5928-35.

36. Hasselbalch, S.G., et al., *Brain Metabolism during Short-Term Starvation in Humans.* Journal of Cerebral Blood Flow & Metabolism, 1994. **14**(1): p. 125-131.

37. Owen, O.E., et al., *Brain metabolism during fasting.* The Journal of clinical investigation, 1967. **46**(10): p. 1589-1595.

38. Pellerin, L. and P.J. Magistretti, *Glutamate uptake into astrocytes stimulates aerobic glycolysis: a mechanism coupling neuronal activity to glucose utilization.* Proc Natl Acad Sci U S A, 1994. **91**(22): p. 10625-9.

39. Bak, L.K., et al., *Neuronal glucose but not lactate utilization is positively correlated with NMDA-induced neurotransmission and fluctuations in cytosolic Ca2+ levels.* J Neurochem, 2009. **109 Suppl 1**: p. 87-93.

40. Bordone, M.P., et al., *The energetic brain - A review from students to students.* J Neurochem, 2019. **151**(2): p. 139-165.

41. Mestre, H., et al., *Aquaporin-4-dependent glymphatic solute transport in the rodent brain.* Elife, 2018. **7**.

42. Zador, Z., et al., *Role of aquaporin-4 in cerebral edema and stroke.* Handb Exp Pharmacol, 2009(190): p. 159-70.

43. Dziedzic, T., et al., *Intracerebral hemorrhage triggers interleukin-6 and interleukin-10 release in blood.* Stroke, 2002. **33**(9): p. 2334-5.

44. Gurney, K.J., E.Y. Estrada, and G.A. Rosenberg, *Blood-brain barrier disruption by stromelysin-1 facilitates neutrophil infiltration in neuroinflammation.* Neurobiol Dis, 2006. **23**(1): p. 87-96.

45. de Oliveira Manoel, A.L., et al., *The critical care management of poor-grade subarachnoid haemorrhage.* Crit Care, 2016. **20**: p. 21.

46. Hu, X., et al., *Cerebral Vascular Disease and Neurovascular Injury in Ischemic Stroke.* Circ Res, 2017. **120**(3): p. 449-471.

47. Suzuki, Y., N. Nagai, and K. Umemura, *A Review of the Mechanisms of Blood-Brain Barrier Permeability by Tissue-Type Plasminogen Activator Treatment for Cerebral Ischemia.* Frontiers in cellular neuroscience, 2016. **10**: p. 2-2.

48. Bardehle, S., V.A. Rafalski, and K. Akassoglou, *Breaking boundaries-coagulation and fibrinolysis at the neurovascular interface.* Front Cell Neurosci, 2015. **9**: p. 354.

49. Rohde, V., et al., *Fibrinolysis therapy achieved with tissue plasminogen activator and aspiration of the liquefied clot after experimental intracerebral hemorrhage: rapid reduction in hematoma volume but intensification of delayed edema formation.* J Neurosurg, 2002. **97**(4): p. 954-62.

50. Turner, R.J. and F.R. Sharp, *Implications of MMP9 for Blood Brain Barrier Disruption and Hemorrhagic Transformation Following Ischemic Stroke.* Frontiers in cellular neuroscience, 2016. **10**: p. 56-56.

51. Ma, Y., et al., *The biphasic function of microglia in ischemic stroke.* Prog Neurobiol, 2017. **157**: p. 247-272.

52. Duan, X., et al., *Intracerebral Hemorrhage, Oxidative Stress, and Antioxidant Therapy.* Oxidative medicine and cellular longevity, 2016. **2016**: p. 1203285-1203285.

53. Qu, J., et al., *The Injury and Therapy of Reactive Oxygen Species in Intracerebral Hemorrhage Looking at Mitochondria.* Oxidative medicine and cellular longevity, 2016. **2016**: p. 2592935-2592935.

54. Ciappelloni, S., et al., *Aquaporin-4 Surface Trafficking Regulates Astrocytic Process Motility and Synaptic Activity in Health and Autoimmune Disease.* Cell Rep, 2019. **27**(13): p. 3860-3872.e4.

55. Salman, M.M., et al., *Hypothermia increases aquaporin 4 (AQP4) plasma membrane abundance in human primary cortical astrocytes via a calcium/transient receptor potential vanilloid 4 (TRPV4)- and calmodulin-mediated mechanism.* The European journal of neuroscience, 2017. **46**(9): p. 2542-2547.

56. Naval, N.S., et al., *An association of prior statin use with decreased perihematomal edema.* Neurocrit Care, 2008. **8**(1): p. 13-8.

57. Chen, Y., et al., *Endothelial NO synthase and reactive oxygen species mediated effect of simvastatin on vessel structure and function: pleiotropic and dose-dependent effect on tumor vascular stabilization.* Int J Oncol, 2013. **42**(4): p. 1325-36.

58. Witsch, J., et al., *Statins and perihemorrhagic edema in patients with spontaneous intracerebral hemorrhage.* Neurology, 2019. **92**(18): p. e2145-e2149.

59. Simard, J.M., et al., *Does inhibiting Sur1 complement rt-PA in cerebral ischemia?* Annals of the New York Academy of Sciences, 2012. **1268**: p. 95-107.

60. Verkman, A.S., M.O. Anderson, and M.C. Papadopoulos, *Aquaporins: important but elusive drug targets.* Nat Rev Drug Discov, 2014. **13**(4): p. 259-77.

61. Abir-Awan, M., et al., *Inhibitors of Mammalian Aquaporin Water Channels.* International journal of molecular sciences, 2019. **20**(7): p. 1589.

62. Kitchen, P., et al., *Identification and Molecular Mechanisms of the Rapid Tonicity-induced Relocalization of the Aquaporin 4 Channel.* J Biol Chem, 2015. **290**(27): p. 16873-81.

63. Verkman, A.S., et al., *The aquaporin-4 water channel as a potential drug target in neurological disorders.* Expert opinion on therapeutic targets, 2017. **21**(12): p. 1161-1170.

64. Salman, M.M., et al., *Design and Validation of a Human Brain Endothelial Microvessel-on-a-Chip Open Microfluidic Model Enabling Advanced Optical Imaging.* Front Bioeng Biotechnol, 2020. **8**: p. 573775.

65. Wevers, N.R., et al., *A perfused human blood-brain barrier on-a-chip for high-throughput assessment of barrier function and antibody transport.* Fluids Barriers CNS, 2018. **15**(1): p. 23.

66. Aldewachi, H., et al., *High-Throughput Screening Platforms in the Discovery of Novel Drugs for Neurodegenerative Diseases.* Bioengineering (Basel), 2021. **8**(2).

67. Salman, M.M., et al., *Advances in Applying Computer-Aided Drug Design for Neurodegenerative Diseases.* International Journal of Molecular Sciences, 2021. **22**(9): p. 4688.

감사의 글

스물 넷 부터 시작했던 대학원 생활이 끝이 났습니다. 4년전 다시 연구를 지속할 수 있게 해주신 이승주 교수님께 먼저 감사의 인사를 드립니다. 교수님 처음 뵈었을 때 성실함만 가지고 있으면 된다고 말씀해 주셨고 항상 많은 칭찬과 조언해 주셔서 4년이 지난 지금 많이 변화한 저를 발견하게 되었습니다. 모든 것이 처음이었기에 지금까지의 과정들이 쉽지는 않았지만 좋은 결과물을 얻게 해 주셔서 감사합니다. 남들과 비교할 것은 아니지만 저는 정말 좋은 시기에 이곳에 왔고 많이 배웠습니다. 교수님께서는 아무것도 없을 때부터 왔다고 하시지만, 그 시간은 저에게 가장 소중한 연구의 기반이 되는 시간이었어요. 제가 이곳에 오지 않았더라면, 저는 아직도 저의 부족한 점만 찾는 사람으로 살았을 것 같아요. 앞으로 저는 교수님께서 주신 가르침을 바탕으로 그동안 준비해온 여러 연구들의 좋은 결실을 거둘 수 있도록 노력하겠습니다. 그리고 바쁘신 와중에도 시간 내어 학위논문 심사에 참여하여 주시고, 그동안 진행한 연구를 되돌아볼 수 있도록 많은 조언해 주신 박원형교수님, 이준엽교수님, 이은재교수님 그리고 조성우 교수님께도 감사의 말씀드립니다.

처음 연구실에 왔을 때, 저에게 하고싶은 일, 연구하면 된다고 저를 배려해준 은엽선생님 원하는 결과가 안나와 속상해 할 때, 뜻대로 되지 않아 예민해져 있을 때 항상 옆에서 흔들림 없이 제 이야기 잘 들어주고 한편으로는 무던하게 넘길 수 있게 도와 주셔서 감사합니다. 밤새서 실험하고 기숙사로 같이 퇴근했던 시간들도 새벽에 출장 간다고 햄버거 먹으며 실험하러 갔던 날들도 지나고 보니 한편으로는 그리운 시간이에요. 초반에 교수님 이랑 셋이 함께 보낸 시간들이 저에게는 너무 소중한 시간이었고 그동안 상처로 자리잡고 있었던 과거의 시간들을 치유할 수 있는 시간이었어요. 그 시간이 저에게는 영원히 기억될 시간일 것 같아요. 실험실을 떠나고 나서도 변함없이 이런저런 이야기도 많이 들어주어서 감사합니다. 저를 이곳에 추천해주시고 많은 도움 주신 양한나 박사님 지금은 다른 곳에 있지만 저의 장점을 발견해주시고 저를 추천해 주셔서 감사합니다. 저도 누군가가 추천할 수 있는 사람이라는 것을 선생님을 통해서 처음 경험하였었는데, 선생님 덕분에 좋은 연구실에서 학위를 얻게 된 것 같습니다. 이 외에도 항상 걱정으로 가득한 저를 잘 챙겨 주시는 정희선생님, 소영선생님 그리고 혜욱선생님, 민정선생님에게도 감사의 마음을 전합니다. 다른 연구실이지만 무슨 일은 없는지 잘 지내는지 항상 먼저 챙겨 주시

는 김진선박사님, 정유선박사님, 김민서박사님, 정지혜박사님, 김지혜박사님, 민교선생님 그리고 새로운 시작을 준비하는 수진선생님 에게도 감사함을 전합니다. 지금은 교수님이 되신 정연 선생님, 석사 때부터 연구실 후배인 것처럼 많은 도움 주시고 미국에 계실 때도 그리고 교수가 되시고 나서도 제 소식 들으시고 항상 응원해 주셔서 감사합니다.

대학교때부터 대학원을 지나 지금까지 매일 아침 서로의 연락으로 하루를 시작 하게하는 은솔이, 그리고 대학교때부터 한 번도 싸운 적 없이 10년 넘게 항상 곁에서 있어주는 나의 친구들 수미, 혜진이, 현주, 효경이, 그리고 석사 때부터 항상 밝은 기운을 전해주는 슬기 에게도 고마움을 전합니다. 자주 보지는 못하지만 언제 만나도 힘이 되어주는 사람들이 있어 힘들었던 시간을 버틸 수 있었습니다. 마지막으로 지금까지 항상 저의 버팀목이 되어주는 가족들, 논문이 되고 나서부터 매일매일 행복함으로 하루를 보내는 엄마와 아빠, 동생들에게 고마움을 전합니다.

저는 남들보다 느리지만 대학교때부터 꿈꿔왔고 한편으로는 이루지 못할 것 같았던 박사라는 결실을 얻었습니다. 앞으로도 저는 처음 마음가짐을 잃지 않고 박사학위에 부끄럼 없이 연구하는 연구자가 되도록 노력하겠습니다.

2021년

전한울 올림

국문 초록

출혈성 뇌졸중은 뇌 실질 내에 생기는 출혈로 고혈압 또는 외부로부터 오는 외상에 의해 유발된다. 이는 높은 사망률 및 2차적 뇌손상을 통한 후유증을 가지는 질병으로 혈압조절 및 뇌압의 조절이 중요하다. 출혈이후 혈종 주변부위에 형성되는 뇌 부종은 향후 환자의 예후에 큰 영향을 미치며, 약물 치료가 불가능한 환자의 경우에는 외과적 수술을 통해 뇌압을 낮추고, 뇌 부종을 치료할 수 있다. 뇌 부종은 활성산소의 증가, 성상세포 water channel의 이상 및 뇌의 대식세포라 불리는 microglia의 활성화, 적혈구의 용혈현상 등이 원인으로 알려져 있다. 뇌 부종으로 인해 신경세포가 사멸하거나 혈-뇌 장벽의 손상이 진행되기 대문에 이를 빠른 시간 내에 최소화할 수 있는 치료법을 찾는 것이 중요하다.

본 연구에서는 자가혈액주입 출혈성 뇌졸중 동물모델 제작 이후 활성산소 제거제 투여를 통해 혈-뇌 장벽의 손상 억제 및 뇌 부종 감소 효과가 나타나는지 확인하고 생존율에 영향을 미치는지 확인하였다. 또한 혈-뇌 장벽의 구성요소 중 하나인 성상세포에 뇌 내의 출혈 이후 환경과 유사한 환경을 유도하여 성상세포에 존재하는 ion 및 water channel의 변화를 확인하고 출혈 이후 해당 세포 및 채널이 질병의 개선에 어떠한 영향을 미치는지 확인하였다. 동물 모델의 평가는 자기공명영상 촬영을 통해 혈종 및 뇌 부종의 크기를 측정하였다. 측정한 동물의 생존율 및 예후 확인을 통해 활성산소 제거제의 뇌 부종 감소 효과를 확인하였으며, 성상세포에 발현하고 있다고 알려진 water channel중 하나인 AQP4 기능에 관하여 확인하였다.

뇌 부종 형성 이후 혈-뇌 장벽을 구성하고 있는 혈관주위세포, 성상세포, 기저막, 밀착 연접의 손상 및 혈관 투과성의 증가가 관찰되었으며 활성산소 제거제 투

여가 혈-뇌 장벽의 기능이 회복에 도움이 되는것을 확인하였다. 또한 유전적으로 AQP4가 결손 된 마우스에서는 혈종 주변의 부종이 더 크게 관찰되는 양상을 확인할 수 있었고, 생존율 감소가 관찰되었다. 우리의 연구 결과는 출혈성 뇌졸중 이후 형성된 출혈 주변부위 부종에 있어 AQP4가 혈-뇌 장벽을 조절할 수 있는 요소임을 발견하였으며 이후 약물 개발에 있어 AQP4 조절제가 혈-뇌장벽의 기능 개선 및 뇌 부종의 감소에 도움이 될 것이라는 것을 시사한다.